A STUDY OF THE $T(d,\gamma)^5He$ REACTION

Thesis by

Peter Andrew Batay-Csorba

In Partial Fulfillment of the Requirements

For the Degree of

Doctor of Philosophy

California Institute of Technology

Pasadena, California

1975

(Submitted May 27, 1975)

ACKNOWLEDGMENTS

I would like to express my gratitude to Professor C. A. Barnes for his encouragement, patience and critical evaluation of this work, and to Professor T. A. Tombrello for his advice, criticism and the many enlightening discussions over the years. It is a pleasure to acknowledge the stimulating and heartening discussions with Professor W. A. Fowler and Professor T. Lauritsen. Each in his own way provided the atmosphere that made my stay at Kellogg enjoyable, challenging and exciting.

I also wish to thank Dr. H. B. Mak and Dr. P. Dyer who introduced me to the time-of-flight measurement techniques, and I am further indebted to Dr. B. D. Anderson for his generous assistance in the frustrating first attempts at the tackling of this experiment.

I am grateful for the many stimulating discussions with Professor A. Winther, Dr. C. Rolfs, Dr. P. Ingalls, Dr. Z. Switowski, and Dr. M. Radomski.

I wish to thank Mr. J. Polchinski, Dr. P. R. Christensen, Mr. G. Fox, and Ms. B. Zimmerman for their assistance in the computer calculations.

Many thanks are offered to all the members of the Kellogg Radiation Laboratory staff for their generous assistance in all phases of this work, and to Mrs. R. Stratton for the skillful typing of this thesis.

I am grateful for the scholarships and the Graduate Research Assistantships from the California Institute of Technology. This

research was supported in part by the National Science Foundation [MPS71-02670 A05].

Finally, Judy and I would like to thank all our friends at Caltech for the many delightful moments we have shared together during all these years.

The labour we delight in
Physics pain.
Shakespeare

ABSTRACT

The cross section for the reaction, $T(d,\gamma)^5He_{g.s.}$, has been measured over the range of deuteron bombarding energies extending from 2 MeV to 12 MeV. A solid ZrT target was employed, and the cross sections were normalized by comparison with the well-known cross sections for the $T(p,\gamma)^4He$ reaction. A well shielded, 8" diameter by 5" long NaI(Tℓ) crystal, 31" from the target, was used to detect the capture γ-radiation. Time-of-flight techniques were employed to suppress cosmic-ray background and neutron background arising mainly from the $T(d,n)^4He$ reaction. Serious pulse pile-up problems were encountered because of an intense flux of lower energy gamma rays arising mainly from contaminants in the target.

For a set of optical model potentials that describe the T + d differential elastic scattering, the direct radiative capture cross section for $T(d,\gamma)^5He$ was calculated. Although the cross section is under-predicted by about a factor of two, the calculated energy dependence of the cross section is similar to that observed.

TABLE OF CONTENTS

I. GENERAL INTRODUCTION

The present experiment was motivated by the gross disagreement among the existing measurements of the $T(d,\gamma)^5He$ reaction (all below 1.3 MeV). There remains considerable interest in the question of how good is the isospin invariance of nuclear forces. In the isospin-mirror reactions $T(d,\gamma)^5He$ and $^3He(d,\gamma)^5Li$, $3/2^+$ states occur near the deuteron thresholds--at E_d = 110 keV in the first reaction and at E_d = 430 keV in the second (Fig. 1). These resonances presumably are members of an isospin doublet. Measurements of the cross section of the reaction $^3He(d,\gamma)^5Li$ have been summarized by King et al. (1972), and the cross section near the $3/2^+$ state seems to be fairly well known. Unfortunately the same cannot be said for the $T(d,\gamma)^5He$ reaction, as will be documented shortly.

Of course, a comparison of the radiative capture cross sections is important at all energies, and measurements of the $D(^3He,\gamma)^5Li$ reaction up to $E_{^3He}$ = 26 MeV (corresponding to an excitation energy in ^5Li of 26 MeV) have been published (King et al. 1972). There are no measurements at all of the $T(d,\gamma)^5He$ reaction for $E_d > 1.3$ MeV, other than the measurements to be presented here (up to E_d = 12 MeV, corresponding to E_x = 24 MeV in ^5He).

The experimental observation that the short-range, two-body nuclear interaction is approximately charge independent (for a given angular momentum state) suggests that one should consider protons and neutrons as charge states of a single particle, the nucleon. Then, to the extent that the contributions due to Coulomb forces and the

neutron-proton mass difference can be neglected, one would expect the binding energies and the energy-level spectra of a collection of A nucleons to be identical regardless of the partition of the A nucleons into N neutrons and Z protons (taking due account of the Pauli principle for identical fermions). With the introduction of the isospin quantum number, a generalized Pauli principle may be stated which requires the antisymmetrization of the A-nucleon wavefunction under interchange of all coordinates, including isospin as well as space and spin coordinates.

The consequences of assuming isospin invariance in the interaction of nuclei with the electromagnetic field has been dealt with in depth by Warburton and Weneser (1969). No details will be given here except to state their Rule 3, that corresponding E1 transitions in conjugate or mirror nuclei (pairs of nuclei for which N and Z are interchanged) have equal strengths (in the long-wavelength limit) whether Δ(isospin) equals 0 or ± 1 . Buss et al. (1963), however, claim a factor of 5 discrepancy in the comparison, at the $3/2^+$ resonances, of the ratio of the experimental cross sections

$$\frac{\sigma_{T(d,\gamma)}}{\sigma_{T(d,n)}} ,$$

with the measured cross section ratio

$$\frac{\sigma_{^3He(d,\gamma)}}{\sigma_{^3He(d,p)}} .$$

The hypothesis of charge independence of nuclear forces predicts very nearly the same value for the above ratios.

However, the previously available $T(d,\gamma)^5He$ data are both incomplete and grossly discordant. The highest bombarding energy measured, prior to the present work, was a thick target (solid) measurement of the $T(d,\gamma)^5He$ reaction between $E_d^{lab} = 0.15$ and 1.3 MeV, using a shielded NaI(Tℓ) detector and normalizing to the $T(p,\gamma)^4He$ cross section (Buss et al. 1963). Their value for the $T(d,\gamma)^5He$ cross section at the 110 keV resonance is 60 μb, and at 470 keV, their results nearly agree with some preliminary thick target data of Coon and Davis (1959). However, as will be evident from the present experiment, the high energy neutrons ($\gtrsim$ 14 MeV) from the $T(d,n)^4He$ reaction may simulate the signals of the high energy photons ($\gtrsim$ 17 MeV) from the $T(d,\gamma)^5He$ reaction.

Kosiara and Willard (1970) did use time-of-flight separation of neutrons and γ-rays for a single measurement at 1.025 MeV. Their value for the cross section of the $T(d,\gamma)^5He$ reaction is about a factor 10 below that deduced by Buss et al. (1963). However, the thin plastic scintillation detector used by Kosiara and Willard suffers from very low γ-ray detection efficiency and essentially no energy resolution, and their technique of accepting all γ-events with pulse-height above a discriminator level of 7 MeV is highly questionable, in light of the serious prompt γ-ray background that may arise from oxygen and nitrogen contaminants in their gas target and from the solid materials of the gas cell.

Bezotosnyi et al. (1970) measured the $T(d,\gamma)^5He$ reaction from 25 to 100 keV using a NaI(Tℓ) detector, and normalizing the cross sections to the neutron yield. Their value for the cross section at the

110 keV resonance is 25 times the resonance $T(d,\gamma)^5He$ cross section reported by Buss. Furthermore, Bezostonyi et al. claim agreement with isospin invariance since their calculated value for the radiative width is

$$\Gamma_\gamma^{T(d,\gamma)} = 14 \pm 4 \text{ eV} \quad ,$$

while that for the mirror reaction is

$$\Gamma_\gamma^{^3He(d,\gamma)} = 11 \pm 2 \text{ eV}$$

(Ajzenberg-Selove and Lauritsen 1974).

The present measurement of the $T(d,\gamma)^5He_{g.s.}$ cross section was undertaken at energies where reasonable pulsed beam currents could be obtained easily, 2 MeV $\leq E_d^{lab} \leq$ 12 MeV, in order to develop the experimental techniques, time-of-flight separation and detector shielding that appear to be necessary for low deuteron energy $T(d,\gamma)$ measurements, as well as for measurements of the $T(d,\gamma)^5He$ reaction at higher deuteron energies. In addition, it is expected that these same techniques will prove useful in the measurement of other γ-ray production cross sections where large neutron backgrounds are encountered.

II. BACKGROUND PROBLEMS AND EXPERIMENTAL METHOD

A. Introduction

The design of this experiment is based on the difficulty in measuring the reaction rate of $T(d,\gamma)\,^{5}He$. The problem lies in separating a small yield of γ-rays above 17 MeV from a very intense background of neutrons (with a range of energies extending from thermal energies to about 20 MeV) and lower energy γ-rays.

NaI(Tℓ) was chosen as the detector because it does not suffer appreciable neutron damage, and has high γ-ray detection efficiency, together with acceptable energy resolution. (The energy resolution is approximately 10% as measured by the 662-keV line of ^{137}Cs). However, because of the long decay constant (1/e) of the light emitted in the NaI (Tℓ) crystal (1/4 μsec), and because of the high event rate in the detector, there is a severe distortion of the pulse-height spectrum because of pulse pile-up: two or more pulses coming so close together in time that they are summed in the subsequent electronics and are stored in the multichannel analyzer as a single event with higher energy. This is a rate-related effect and may be studied by repeating the measurements at different beam currents.

B. Neutron Background

Prompt neutrons with energies from 14 to 20 MeV are produced at the target by the $T(d,n)\,^{4}He$ reaction. The deuteron beam also produces lower energy neutrons when it hits position-defining apertures along its path. These neutrons may scatter many times from the walls of the target room, forming a sea of thermalized (or partially thermalized)

neutrons which fills the target room. Some neutrons are, of course, also produced by interactions of the deuteron beam with the zirconium and platinum in the target, especially at the highest deuteron energies used. These neutrons were always a small fraction of those coming from the tritium and low-Z impurities in the target.

Neutrons may also be captured outside the crystal, with the detection of their subsequent γ-rays. Neutrons coming directly from the target or the beam-defining slits may interact with the NaI crystal in several ways:

(a) neutron capture with the emission of γ-rays with energies up to 8 MeV, producing ^{24}Na or ^{128}I which are γ-emitters with half-lives of 15 hours and 25 minutes, respectively;

(b) the production of γ-rays from the excitation of ^{23}Na and ^{127}I by inelastic neutron scattering;

(c) the production of recoiling ^{23}Na or ^{127}I nuclei by either elastic or inelastic scattering;

(d) the production of both light and heavy nuclear fragments by nuclear reaction with the ^{23}Na and ^{127}I nuclei in the crystal;

(e) any of these processes in the materials which surround the crystal.

The observed pulse-height spectrum looks relatively flat from about 2 MeV to 8 MeV, and then falls rapidly with increasing energy. However, the intensities of the lower-energy events are so high that this rapidly falling tail is still significant in the region of the γ-rays from $T(d,\gamma)\,^{5}He$, mainly because of the pile-up problem alluded to above.

C. Gamma-Ray Background from the Target

A very serious problem is posed in this experiment by γ-rays from (d,γ), (d,pγ), (d,nγ) and (d,$\alpha\gamma$) reactions on oxygen and nitrogen contaminants in the target. Zirconium metal is a good getter for these gases, and the manufacturers of the target appear to have taken insufficient care to avoid contamination of the target by these gases, as will be discussed later. Pile-up of these γ-rays produces a background that is hard to subtract from the γ-rays of interest, and, of course, time-of-flight separation is not feasible for discriminating against these γ-rays.

The presence of carbon, oxygen and nitrogen in the target was verified by measuring the time-of-flight spectrum of the neutrons arising from (d,n) reactions on these target contaminants. Another clear indication of the presence of nitrogen in the target is the detection of 15 MeV γ-rays from the reaction $^{14}N(d,\alpha\gamma)\ ^{12}C$. The excitation function for these γ-rays agrees well with the published energy excitation function of Browne (1965). From the measured yields, the estimated ^{14}N contamination is approximately 0.1% by weight throughout the zirconium layer.

The experimental set-up to be discussed in the following sections utilizes two approaches to minimize the difficulties posed by the intense backgrounds discussed above (Dyer 1973, and references therein):

1) shielding of the detector; and
2) separation by time-of-flight of the γ-rays from the target, from prompt neutrons from the target, prompt neutrons and γ-rays from other locations, and general time-independent background, such as cosmic radiation and thermalized neutrons.

D. Beam Preparation and Time-of-Flight System

Deuterons were accelerated by the ONR-CIT tandem accelerator to energies between 2 and 12 MeV, and protons up to 6 MeV were also employed in detector efficiency and target thickness measurements.

The principal components of the beam-pulsing system (Dietrich 1964) are a "beam-chopper" and a "beam-buncher". The beam-chopper is a set of parallel plates situated at the high-energy end of the accelerator. An r.f. voltage with a frequency of 3.531×10^6 Hz and a magnitude of about 3 kV applied to these plates deflects the beam across a pair of vertical slits (set at ±150 mils) located after the 90° beam-analyzing magnet. The chopping voltage was selected to give beam bursts with a time resolution of approximately 3 nsec FWHM (full width at half maximum). The time-averaged beam current was thereby cut to approximately 1% of its D.C. value. A velocity-modulating system, located before the entrance to the accelerator and operating at the same frequency as the chopper, was then used to form the beam into bunches. The phase and amplitude of the r.f. signal in the buncher was then adjusted in such a way as to allow the maximum current to go through the chopping slits. The time-averaged deuteron beam was typically increased by a factor of 2 to 5 to produce beam currents of from 50 to 150 namp on target.

It was found that the shortest beam bursts on target (best time resolution) were obtained when the beam focusing and steering preceding the 90° analyzing magnet were left unchanged after first maximizing the D.C. beam in the target room. When the beam was then chopped, this procedure allowed the beam to be swept across the chopping slits during the fastest portion of the r.f. waveform.

The set of slits that defines the cross-sectional area of the beam was located 11 ft from the target, far enough away from the detector that neutrons and γ-rays produced at the slits would be separated by their longer time-of-flight from those γ-rays and neutrons from the target. The beam was focused down to a square roughly 1/8" on the side at the center of the target.

E. Target System

The tritium target employed in the present work was a zirconium tritide compound purchased from the Oak Ridge National Laboratories. It was manufactured by vacuum evaporation of 3 mg/cm^2 of zirconium onto a 3.2 cm diameter, 10 mil thick, platinum backing. The target was allowed to cool and then transferred, through the atmosphere, to another evacuated bell jar. Here the zirconium was heated in an atmosphere of tritium gas, allowed to cool, and then shipped to us packaged in argon gas. In our laboratory, the target was always stored under vacuum or in clean argon (less than 0.1% impurities), and exposed to air as little as possible while being transferred to its location in the evacuated target chamber where it was bombarded. As noted above, no attempt was made at the time of manufacture to prevent contamination of the target by the atmosphere. Zirconium is a very good getter for oxygen and nitrogen, and it is probable that most of the absorption of these gases took place during the transfer in air between the two bell jars, although there is also the possibility that the argon used in the packaging of the target was insufficiently pure.

All of the beams used in the experiment go completely through the zirconium layer (of thickness equal to the range of 1/2 MeV deuterons)

and are stopped at the platinum backing.

With a uniform 1:1 ratio of tritium to zirconium atoms in the target, the target contains approximately 100 μgm/cm^2 of tritium. This is in rough agreement with the tritium content of the target as determined by measuring the yield of the $T(p,\gamma)\,^4He$ reaction.

The target was mounted with good thermal contact on a thin copper sheet, the back of which was continually cooled by a blast of air. In addition, the beam intensity was kept below 150 namp to avoid decomposition of the ZrT which is unstable above 150°C. A tritium "sniffer" constantly monitored the exhaust of the diffusion pump to detect any tritium gas released.

The uniformity of the tritium impregnation was confirmed (within the $\sim$5% statistical uncertainty) by measuring the $T(p,\gamma)\,^4He$ yield at various points on the target. In addition, before and after each series of measurements of the $T(d,\gamma)$ reaction, the $T(p,\gamma)\,^4He$ reaction was used to monitor the tritium content. No loss of tritium was detected (within $\sim$3% statistics) before and after each set of runs (typically lasting two days).

A sketch of the experimental set-up is shown in Figure 2. The target was contained in a T-shaped glass target chamber, and was oriented at 45° to the beam direction (during angular distribution measurements the angle was slightly less than 45° to avoid blocking the path to the detector). During the various runs of the experiment, the vacuum was always kept at better than 5×10^{-6} torr to avoid build-up of carbon on the target. Electrons produced at the beam defining slits were prevented

from reaching the target by a suppressor ring biased at -300 volts. The target rod was biased as +300 volts to collect secondary electrons knocked out of the target. The beam collection efficiency was verified by varying the target voltage and bias voltage from 0 to ±1000 V. A battery and known resistor were used to check the current integrator at the settings and currents normally used during the runs.

F. Detection System and Detector Shielding

The detector used was an 8" diameter by 5" long NaI(Tℓ) crystal (Fig.2). More than 85% of the γ-rays with energies above 17 MeV will interact with the crystal in a depth of 5", producing pulses somewhere in the pulse-height spectrum; this detection efficiency was calculated using the mass attenuation coefficients tabulated by Grodstein (1957).

The most effective way to separate the γ-rays from the neutrons emitted from the target was to use the fact that their propagation velocities are quite different, that is, to use time-of-flight (TOF) separation. However, to assist in the separation, the distance (31") between the target and detector was filled with matter that attenuated the 14 to 20 MeV neutrons by a factor of approximately 1000 while attenuating the γ-rays of interest (17 to 24 MeV) by only about a factor of 3. This neutron attenuator was made in the form of a cone to avoid re-scattering into the detector of those fast neutrons which would not otherwise have hit the crystal. The cone was made out of a mixture of paraffin (to thermalize the neutrons) and 25% by weight of B_2O_3 [^{10}B has a high cross section for non-radiative capture of slow neutrons through the $^{10}B(n,\alpha)\ ^{7}Li$ reaction, plotted by Marion and Young (1968)].

Attenuating the prompt neutrons makes the neutron TOF peak comparable in height to the γ-ray TOF peak, in the energy region of interest, allowing cleaner separation. In addition, the total counting rate in the photomultiplier is also reduced, lessening the chances for gain shifts and pulse pile-up.

The NaI was also surrounded on the sides by a thick lead cylinder and in front by a hollow lead cone, to shield the crystal from γ-rays produced by the deuterons striking the beam-defining slits or by radiative neutron-capture on walls, ceiling, floor, and other material around the room. The shielding also reduced the counting rate from high-energy cosmic rays somewhat. A minimum of 5" lead surrounded the detector (except in the back to reduce backscattering of γ-rays and neutrons) to attenuate the γ-rays of any energy by more than a factor of 100. A thin sheet of lead 1/16" thick was placed in front of the detector to reduce the intensity of very low energy γ-rays emanating from the target or produced by the neutrons in the neutron-attenuation cone.

The electronic set-up is sketched in Figure 3 . The scintillation quanta in the crystal were detected with a 13.3 cm diameter RCA type 4522 14-stage photomultiplier tube, chosen for its fast timing capability and good pulse height resolution. The photomultiplier anode signal is used to start a time-to-pulse height converter (TAC) which is then stopped by a signal (from an antenna near the chopper), which is assumed to be accurately related to the time of arrival of beam bursts at the target. This time-of-flight information is stored in a pulse-

height analyzer as the Y-coordinate of a two-dimensional array. Simultaneously, the X-coordinate is derived from the pulse height information in the signals from the 9th dynode of the photomultiplier. This pulse height is linearly proportional to the energy deposited in the NaI crystal. The linearity of the electronics from the pre-amplifer to the analyzer was tested using a sliding pulser before and after each running period.

Moreover, before and after each series of runs with deuterons, the $T(p,\gamma)\ ^4He$ reaction was examined at $E_p^{lab} = 4$ MeV and $\theta_{lab} = 90°$ for three reasons:

1) to obtain a normalization for the $T(d,\gamma)$ yields that would include the tritium target thickness, the detector solid angle, the detection efficiency, and the γ-ray attenuation in the neutron attenuating cone;
2) to determine the energy calibration and energy resolution of the NaI detector; and
3) to determine the pulse-height response of the NaI for monochromatic γ-rays of energy near the energy of the $T(d,\gamma)\ ^5He$ γ-rays. The $T(p,\gamma)$ pulse-height spectrum would then be used (as will be explained later) to simulate (in the computer) the pulse height spectrum of γ-rays to the <u>unbound</u> ground state of ^5He. (Appendix 2).

The $^{11}B(d,n\gamma)\ ^{12}C$ 15.1 MeV γ-rays were also studied frequently to assist in determining the energy calibration and response function for the NaI detector. In addition, the γ-rays from an ^{88}Y source (E_γ = 0.9 and 1.8 MeV) and an $^{241}Am/Be$ source [a compacted mixture of

americium oxide with beryllium metal, which produces 4.44 MeV gamma-rays from the reaction $^{9}Be(\alpha,n\gamma)\ ^{12}C$ occurring inside the source] were also used for energy calibration and to check the linearity of the detector. The $^{241}Am/Be$ source was monitored before and after each $T(d,\gamma)$ and $T(p,\gamma)$ run to check for gain shifts in the photomultiplier and to verify that the detection system from crystal to analyzer was in proper working order.

The energy region in which the yields were extracted lay above 15 MeV. Approximately below this energy, the number of γ-ray counts per unit charge deposited on the target were seen to vary with the beam intensity because of pulse pile-up. Therefore, at each beam energy and detector angle, the measurements were repeated at smaller and smaller currents until no pulse pile-up effect was seen in the yield of γ-rays in the energy region of interest.

An unshielded 5" diameter and 2" thick plastic scintillator detector located 15 ft from the target was also used to monitor the deuteron (or proton) runs being recorded simultaneously in the NaI detector. The rapid accumulation (since there was no attenuating material in front of the plastic detector) of prompt γ-rays (above 1 MeV) in the TOF spectrum of the plastic detector aided in determining the time width (resolution) of the beam, and in adjusting the time delays between the "start" and "stop" signals in the NaI TAC (where timing adjustments were tedious due to the low rates). The plastic scintillator also allowed detection, throughout the course of a run, of time shifts of the stop signal (probably from instabilities in the chopper electronics); when such a time shift was noticed, the analyzer accumulating the NaI data

was cleared and the run restarted.

Sometimes it is possible to have two beam bursts per r.f. cycle reaching the target since the beam is deflected first in one direction and then in the other across the chopping slits. Adjustment of the target room steering controls can prevent one of the beam components from reaching the target, since they have slightly different trajectories through the beam-transport system. To make this adjustment, the existence of this second beam burst (approximately 140 nsec after the first) must be detected. The TOF spectrum from the NaI detector will not reveal it, since the NaI TAC was set for a total range of 100 nsec for good time resolution. Since this second beam component may have, at times, as much as 25% of the intensity of the primary component, and since the γ-rays produced by it are not recorded in the NaI TOF spectrum, an important error may be introduced into the cross section measurements. Therefore, the TOF spectrum of the plastic detector, with a TAC range of 400 nsec, was monitored during all runs and no data were taken until the second beam component was prevented from reaching the target.

The measurements of the proton runs, the $T(p,\gamma)\ ^4He$ reaction for normalizing the deuteron runs, were carried out in as nearly similar manner as the deuteron runs as possible: same beam currents, TOF resolution, energy calibration, and the target position was not changed (to increase the probability that the same spot on the target was bombarded). Deuteron runs alternated with proton runs (each preceded and followed by the monitoring of the 4.44 MeV gamma rays from an $^{241}Am/Be$ source), but the detection system and electronics were not changed.

III. ANALYSIS OF THE DATA

A. Extraction of the γ-Ray Yields

The data were stored in the pulse-height analyzer in a 64 x 64 channel array: time-of-flight vs. pulse-height. Spectra were then plotted in one dimension after choosing a window in the other dimension.

Monoenergetic γ-rays interacting in the NaI crystal give rise to a pulse-height spectrum which extends all the way from zero energy to slightly above the energy of the γ-rays. The energy resolution (FWHM) for 21 MeV γ-rays (Figure 4) was about 20%, a value typical of the γ-rays in the region of interest, 15 MeV $\leq E_\gamma \leq$ 25 MeV. The broadening of the peak was caused by the escape from the crystal of bremsstrahlung photons from the electrons and positrons created through pair production by the primary γ-ray.

In the present experiment, the pulse-height spectrum of γ-rays from deuteron bombardment of the ZrT target showed an intense background of low-energy pulses which fell rapidly above 12 MeV, and a broad peak where the "photopeak" from the $T(d,\gamma)\ ^5He_{g.s.}$ reaction is expected on the basis of the pulse-height calibration and kinematic calculations. Only the portion of the spectrum lying above 0.8 E_γ^o , where E_γ^o is the central energy of the γ-ray being measured, was reasonably above the tail of the low-energy background (Figure 5). Above 1.1 E_γ^o the pulse-height spectrum of the γ-rays has come down to a nearly flat, time-independent, high-energy background, from cosmic radiation.

At some energies, however, the lower end of the energy region of interest was taken at 0.9 E_γ^o to avoid including any of the 15.1 MeV γ-rays

from the $^{14}N(d,\alpha\gamma)\ ^{12}C$ reaction.

When the low-energy background was extrapolated smoothly into the energy window, it was found to contribute less than 10% to the total counting rate inside the energy window.

The time-of-flight spectrum was then plotted for all pulses lying within the energy region of interest. Typical spectra are shown in Figure 6 . The time-of-flight spectra due to the prompt neutrons [from $T(d,n)\ ^4He$] or the γ-rays could be readily obtained separately by selectively attenuating one or the other radiation by interposing additional amounts of paraffin or lead between the target and detector. Furthermore, the time separation between the well-separated peaks agrees with that calculated from the energy of the fast neutrons and the target-to-detector distance. As further confirmation of the separation of the neutrons and the γ-rays, the yield under the neutron TOF peak follows the published (Marion and Fowler 1960) angular distributions for the $T(d,n)^4He$ reaction. The distance to the detector was, of course, determined by the requirement of a clean separation between the γ-rays and prompt neutrons.

The only other feature seen in the TOF spectra is a flat background (independent of time) produced by cosmic rays and the sea of neutrons that pervades the room. These neutrons, produced at the target or at beam defining slits, have bounced around the room and have lost all the time correlation by the time they (or their capture γ-rays) are detected in the NaI.

All data quoted in this thesis are taken from runs in which the prompt neutrons were cleanly separated from the γ-rays, and from runs in

which the γ-rays were seen not to depend on the magnitude of the beam current.

The linear response and the energy calibration of the detector was established by looking at the γ-rays from the ^{88}Y and $^{241}Am/Be$ sources and from the $^{11}B(d,n)^{12}C^*_{15.1MeV}$ and $T(p,\gamma)^4He$ reactions. At each bombarding energy and detector angle, the energy of the γ-ray of interest (E^o_γ) to the central position of the ground state of ^5He (Q = 16.7 MeV) was then calculated by means of a relativistic kinematics calculation (Marion and Young 1968). The energy window of interest ($0.8E^o_\gamma \leq E \leq 1.1E^o_\gamma$) was then determined from the energy calibration of the detector, and the TOF spectrum was plotted for events inside this energy window.

The yield of γ-rays from the $T(d,\gamma)^5He$ and $T(p,\gamma)^4He$ reaction in the energy region of interest ($0.8E^o_\gamma$ to $1.1E^o_\gamma$) was obtained by counting the number of events inside the γ-ray TOF peak, and subtracting the time-independent background underlying the peak (estimated by extrapolating a horizontal line drawn through the data corresponding to times before the arrival of the γ-rays).

The experimental arrangements for the deuteron and proton runs, as well as the extraction of the γ-ray yields, were carried out, as nearly as possible, in the same manner.

B. NaI(Tℓ) Detection Efficiency

Detection response of the 8"x5" NaI(Tℓ) crystal as a function of energy and geometry was determined by performing numerical integrals of the following form (Lazar et al. 1956):

$$J_n = \frac{1}{2\pi} \int_{\text{crystal}} P_n \, e^{-\mu_1 \ell_1} (1 - e^{-\mu_2 \ell_2}) \, d\Omega' \quad .$$

For a system with axial symmetry this becomes

$$J_n = \int_{\text{crystal}} P_n(\cos\theta') \, e^{-\mu_1(E)\ell_1(\theta')} (1 - e^{-\mu_2(E)\ell_2(\theta')}) \sin\theta' d\theta' \, ,$$

where $P_n(\cos\theta')$ is the Legendre polynomial of order n ;

$\ell_1(\theta')$ is the gamma ray path length in absorbing medium preceding the NaI(Tℓ) crystal;

$\mu_1(E)$ is the linear attenuation coefficient for a gamma ray in the absorbing medium: paraffin + B_2O_3 cone, glass-T, 1/16" lead disk, and steel housing and Al_2O_3 reflector of the crystal;

$\ell_2(\theta')$ is the gamma ray path length in NaI(Tℓ);

$\mu_2(E)$ is the linear attenuation coefficient for a gamma ray in the NaI(Tℓ) detector;

$E = E_\gamma^o$ is the gamma ray energy calculated at each bombarding energy and detector angle, θ'; and

θ' is the laboratory angle of the gamma ray with respect to the symmetry axis of the detector (the source is assumed to lie on the symmetry axis of the detector, defined as $\theta' = 0$).

The linear attenuation coefficients $\mu(E)$ are available in tabulated form for a variety of materials (Grodstein 1957).

The detection efficiency, ε , defined as that fraction of γ-rays emitted by an isotropic point source which interacts with the detector giving rise to a signal anywhere in the pulse height spectrum, is given by the integral $J_o/2$. For the case of maximum γ-ray absorption in the crystal ($e^{-\mu_2 \ell_2} = 0$) and no absorber preceding the crystal ($\mu_1 = 0$),

$$\frac{J_o}{2} \rightarrow \frac{1}{4\pi} \int_{\text{crystal}} d\Omega' \quad .$$

Therefore, in general, the detection efficiency, $\varepsilon = J_o/2$, is a measure of the fraction of the solid angle subtended by the detector with appropriate modifications due to detector efficiency and γ-ray attenuation in the material before the detector.

By a suitable coordinate transformation, Rose (1953) has demonstrated that the integrals J_n form a simple relationship between the axial coordinate system of the detector (designated here by primes) and the coordinate system defined by the incident projectile particle and emerging gamma ray. For an emitted γ-ray angular distribution of the form

$$W(\theta) = \sum_n A_n P_n(\cos\ \theta),$$

where θ is the angle of the γ-ray relative to the direction of the incident particle beam,

a detector subtending a finite solid angle will measure the distribution $(J_o/2)W(\theta)_{obs}$, where (see Pearson 1963 Appendix A, and Ferguson 1965)

$$W(\theta)_{obs} = \sum_n A_n Q_n P_n(\cos\theta) \quad ,$$

$$Q_n \equiv J_n/J_o \quad , \qquad Q_n \leq 1 \quad .$$

The quantities Q_n are Rose's attenuation factors; in effect they describe the detector response to higher order polynomial terms in the angular distribution. These factors tend generally to decrease with increasing n, producing a less rapidly varying angular dependence, or "smoothing", of the observed angular distribution. For two γ-ray energies in this experiment, the values of $J_o/2$ and Q_n for the 8"x5" NaI(Tℓ) detector are given in Table 1.

C. Calculation of the Differential Cross Section

To avoid the measurement of the amount of tritium in the target and to minimize the error in calculating the detection efficiency and cone attenuation, the cross section for the $T(d,\gamma)^5He$ reaction was calculated by normalizing to the yield of the $T(p,\gamma)^4He$ reaction in the following way:

$$\frac{d\sigma_d}{d\Omega} = \frac{Y_d}{\varepsilon_d Q_d f_d} * \frac{\varepsilon_p Q_p f_p}{Y_p} * \frac{d\sigma_p}{d\Omega}$$

where the subscripts d and p refer to the $T(d,\gamma)^5He$ and $T(p,\gamma)^4He$ runs respectively, and where

Y is the number of counts in the TOF γ-ray peak (above the time-independent background) and in the energy region of interest ($0.8E_\gamma^o$ to $1.1E_\gamma^o$) ;

$\frac{d\sigma_p}{d\Omega}$ is the differential cross section of $T(p,\gamma)^4He$ at $E_p^{lab} = 4$ MeV and $\theta_{lab} = 90°$. The value, as published by Meyerhof et al. (1970) is 9.78 μb/sr (± 2%);

Q is the total charge deposited on the target during the analyzer "live-time";

ε includes the solid angle, detection efficiency and attenuation of γ-rays in the absorbing medium (Table 2)

$$\varepsilon \equiv \frac{J_o}{2} = \int_{crystal} d\Omega \, [e^{-\mu_1 \ell_1}(1 - e^{-\mu_2 \ell_2})] \; ;$$

f is the "spectrum fraction"--the fraction of the total area under the pulse-height spectrum that lies inside the energy region of interest: $0.8E_\gamma^o$ to $1.1E_\gamma^o$. The spectrum fraction for monochromatic γ-rays from 15 to 24 MeV was measured using the $B(d,n\gamma)^{12}C$ and $T(p,\gamma)^4He$ reactions. No significant energy dependence was found (see Table 3) and the average value was 0.40 ± .02. The γ-rays from $T(d,\gamma)^5He$ are not monochromatic, since the ground state of ^5He is unbound with respect to α+n decay with a width $\Gamma_{cm} \simeq 0.6$ MeV. The pulse height spectrum was therefore simulated by using a theoretical line shape derived mainly from the phase shift of α+n (see Appendix 2). The results are tabulated in Table 4. The spectrum fractions for the simulated pulse height spectra of $T(d,\gamma)^5He_{g.s.}$ γ-rays in the range 17 MeV $< E_\gamma <$ 24 MeV were seen to vary by less than 5%. Thus in the cross sections quoted, f_d was taken equal to f_p at all energies because 1) the large rates of low energy γ-rays made it difficult to extrapolate the monochromatic γ-ray pulse height spectrum to zero energy, and thus to determine the energy dependence of the spectrum fraction, and 2) the width of the ground state of ^5He did not appreciably

broaden the spectrum. Simulations were also carried out for equal probabilities for transitions to the ground state and the first excited state, but the spectrum fraction for ground state transitions was not appreciably changed, since the γ-rays to the first excited level are of sufficiently lower energy that they do not appear inside the ground-state energy window with significant probability.

All of the $T(d,\gamma)$ runs were normalized only to those $T(p,\gamma)^4He$ yields at E_p = 4 MeV and θ_{lab} = 90°. However, as a check on the detection system, charge collection and yield extraction, the $T(p,\gamma)^4He$ reaction was also measured at E_p^{lab} = 1.5, 3 and 6 MeV, and an angular distribution measured at 4 MeV. The measured shape of the $T(p,\gamma)^4He$ 90° excitation function is in good agreement with the published results of Perry and Bame (1955) and Meyerhof et al. (1970). The absolute value of the $T(p,\gamma)$ cross sections is only in rough agreement (within 25%), presumably because of the uncertainty in the amount of tritium in our target.

The differential cross section of $T(d,\gamma_0)^5He$ at 90° is plotted in Figs. 7 and 8 along with some of the results from a previous study of $D(^3He,\gamma_0)^5Li$ (King et al. 1972), plotted at the same excitation energy of the compound nucleus.

The cross sections for the two mirror reactions agree quite well within the error bars, although the $T(d,\gamma_0)^5He$ cross sections appear to peak 1 to 2 MeV higher in energy.

D. Angular Distributions

1. Measurement

Wheels were installed under the detector cart allowing quick and easy change of angles. The center of rotation of the detector at a fixed radius was adjusted (by telescope) to intersect the beam axis. Thus, the detection system consisted of an 8"x5" NaI(Tℓ) crystal which 1) could be rotated about the glass-T target holder continuously from -45° to +140°; 2) was shielded on the sides by at least 5" of lead; 3) was at a distance from the target that could be varied continuously from 1 ft to 4 ft (31" was used for this experiment); and 4) was shielded in front by a conical lead collimator filled with boron-loaded paraffin.

Yields were measured at θ_{lab} = 0, 45, 90, and 135°, and at E_d^{lab} = 4, 8, 10, and 12 MeV.

No changes in the experimental set-up were made for the angular distribution measurements, except to remove 11" of the lead collimator nearest to the target to facilitate back angle measurements; however, the boron-loaded paraffin cone was left in place (propped up so as not to interfere with the change of angles); no effect was noticed due to the removal of the front pieces of the collimator . Once the beam was focused on target, the measurements at all detector angles were done without changing the target position and without refocusing or steering the beam to make sure that the same spot on the target was bombarded. Of course, the beam instabilities may make the spot wander, but these fluctuations in position are thought to be negligible in light of the

measured uniformity of the target. $T(p,\gamma)^4He$ yields, measured 1/4" above and 1/4" below the usual spot bombarded, agreed within statistics (5%).

Measurements at each angle were repeated after halving the beam current to test for pulse pile-up.

After runs at all four angles were completed, the measurements were redone to check reproducibility. These agreed in all cases within statistics.

The yields of $T(p,\gamma)^4He$ measured at $\theta_{lab} = 45°$ and $\theta_{lab} = -45°$ (other side of the beam line) agreed within the 5% statistical uncertainty. These runs were carried out to check the zero degree position of the angle scale, which is not expected to be very critical, considering the 15° opening angle of the NaI crystal. However, such runs on either side of the beam would uncover a left-right asymmetry in the detection apparatus if it were present.

The yields of the angular distribution were extracted from the γ-peak in the TOF spectra in the same manner as the yields of the 90° excitation function. At $\theta_{lab} = 0°$, additional corrections were required for the γ-ray attenuation through the target backing and the target holder (see Table 2).

The yields of the angular distribution were extracted from the γ-peak in the TOF spectra ($0.8E_\gamma^o \leq E_\gamma \leq 1.1E_\gamma^o$) in the manner discussed previously.

2. Fitting with Legendre Polynomials

From each run, the yield of γ-rays per micro-Coulomb of beam charge was extracted and divided by $\varepsilon = J_o/2$. The yields at $\theta = 0°$

were further corrected by about 10% for attenuation in the target and the target holder. The yields and angles were then transformed to the d + T center-of-mass (CM) coordinate system (Williams 1964) before being fitted with Legendre polynomials:

$$W_{obs}(\theta_{CM}) = \sum_n A_n Q_n P_n(\cos \theta_{CM})$$

where $Q_n = J_n/J_o$ are Rose's attenuation factors, discussed above, to describe the corrections to the angular distribution due to the finite size of the detector.

A check on the measurement of the angular distribution was made by looking at the $T(p,\gamma)^4He$ reaction at E_p = 4 MeV and θ_{lab} = 0°, 45°, 90°, 135°. These yields were transformed to the p + T CM system and treated in the same manner as the $T(d,\gamma)$ runs. The 45° and 135° yields agreed within statistical precision ($\sim$ 3%), thus showing no forward-backward asymmetry in the detector. The $T(p,\gamma)^4He$ angular distribution was well fitted by $\sin^2\theta$ in agreement with the results of Perry and Bame (1955).

In Figure 9 are shown the experimental angular distributions for $T(d,\gamma_o)^5He$ and $T(p,\gamma)^4He$, along with the Legendre polynomial fits to the data using only A_o and A_2 terms. In general, even polynomials alone provided reasonable fits (A_4 terms were found to be not necessary). However, there is evidence for a small asymmetry about 90° in the CM yields, particularly at the higher excitation energies investigated. Table 5 shows the results of the Legendre fits using only even polynomials (A_o and A_2), or both even and odd polynomials (A_o, A_1 and A_2).

In Figure 8, the experimentally determined ratio, A_2/A_o for the $T(d,\gamma_o)^5He$ and $^3He(d,\gamma_o)^5Li$ reactions is plotted as a function of the excitation energy in the compound nucleus $[E_x(^5A)]$. At excitation energies below approximately 18 MeV, the cross section is nearly isotropic (A_2/A_o is zero). Above 20 MeV the ratio steadily decreases and appears to level out at approximately $A_2/A_o = -1/2$.

The total cross sections were calculated from the results of the fits using only A_o and A_2. At those energies in which angular distributions were not measured, smooth interpolations were made of the A_2/A_o curve (Figure 8). The total cross sections thus obtained are plotted in Figure 11 with only statistical error bars, and compared to theoretical calculations of the E1 direct capture component.

E. Sources of Error

1. Yields

The γ-ray yields for the $T(d,\gamma_0)^5He$ reaction are given by

$$Y_d = Y_\gamma - Y_B$$

where

$$Y_B = \frac{Y_{ind}}{c_{ind}} * c_\gamma$$

and Y_γ is the sum of the counts under the γ-ray peak in the TOF spectrum for $0.8E_\gamma^o \leq E \leq 1.1E_\gamma^o$;

Y_B is the background under the γ-ray peak ;

Y_{ind} is the sum of the counts in the time-independent background (Figure 6); and

c_γ and c_{ind} are the number of analyzer channels in the region of the γ-ray peak and the time-independent background, respectively.

The area (A) is the sum of the counts/channel (y_i) over a specified region,

$$A = \sum y_i$$

The statistical uncertainty (Δ) in the counts per channel is given by the Poisson statistics:

$$\Delta y_i = \sqrt{y_i}$$

Therefore,

$$\Delta A = \sqrt{\Sigma(\Delta y_i)^2}$$

$$= \sqrt{\Sigma y_i}$$

$$= \sqrt{A}$$

Thus, the statistical error in the extracted γ-ray yields is given by

$$\Delta Y_d = \sqrt{(\Delta Y_\gamma)^2 + (\Delta Y_B)^2}$$

$$= \sqrt{Y_\gamma + \frac{c_\gamma}{c_{ind}} Y_{ind}}$$

The value of $\Delta Y_d/Y_d$ is typically 10% or less for the $T(d,\gamma)^5He$ measurements. The $T(p,\gamma)^4He$ yields have a statistical error, $\Delta Y_p/Y_p$, usually less than 3%.

2. Normalization

The cross section normalization factor, $\frac{d\sigma_p/d\Omega}{Y_p}$, has been assigned an error of ±5%. This error includes the statistics in the measurement of the $T(p,\gamma)^4He$ yield, the uncertainties in the published cross sections (2 %, Meyerhof et al. 1970), and the uncertainties in the target non-uniformity (discussed later), in the target centering and in the wandering of the beam spot on the target.

3. Solid Angle

The target-to-detector distance was determined to better than 1% accuracy (less than 1/4" out of 31"). The actual size of the NaI crystal inside the steel casing is not available; but the accuracy of the solid angle is estimated to be better than 3%.

Solid angle corrections arising from Compton scattering of γ-rays from the lead cone into the crystal are negligible since, at the energies measured, only 12% of all γ-ray interactions go by Compton scattering. In any

case, the solid angle for T(d,γ) runs cancels out with the normalization to the T(p,γ) runs which have γ-rays of nearly equal energies.

4. Bombarding Energy

The beam energy from the tandem is analyzed to ±20 keV at the 90° bending magnet.

The maximum energy loss of the deuteron beam in the ZrT target is 0.4 MeV at 2 MeV bombarding energy; 4 MeV protons lose 0.14 MeV.

5. Gamma Ray Attenuation

The assigned error in the γ-ray attenuation ($e^{-\mu_1 \ell_1}$) in the boron-paraffin cone is ±10%. This includes the uncertainties in the tabulated mass attenuation coefficients (Grodstein 1957), the B_2O_3 and paraffin densities, and the thickness of the material.

6. Detector Efficiency

The error in the NaI detection efficiency ($1 - e^{-\mu_2 \ell_2}$) is ± 3% on the basis of the accuracy of the attenuation coefficients, the NaI density, and the detector size.

7. Charge Integration and Electronic Dead-Time

The error in the charge integration is less than 1% as determined by battery measurements. The charge collection efficiency was checked by varying the suppressor and target biases. The analyzer dead-time was kept at less than 5%.

Some errors in charge integration would have shown up in the remeasurement of the 4 MeV yield of the $T(p,\gamma)^4He$ reaction. The γ-ray yields always agreed within the 3% statistics.

The $T(d,\gamma)$ yields remeasured for consistency checks through the duration of the experiment agreed within 10% statistics. The vacuum in the beam line from the 90° analyzing magnet to the target was kept below 7×10^{-6}torr; therefore, no significant uncertainty in the effective charge of the beam is expected.

8. E_γ^o

The mean energy of the γ-rays to the central position of the unbound ground state of $^5He(\Gamma_{CM} \sim 0.6$ MeV) was calculated from relativistic kinematics using the tabulated masses of the particles and the energy of the beam at the middle of the target. The uncertainty in E_γ^o is estimated to make a negligible contribution to the extracted γ-ray yields or to the value of the absorber attenuation or detection efficiency.

9. Detector Calibration and Linearity

The linearity of the electronics was better than 2% as tested by connecting a sliding pulser at the preamplifier test input and accumulating the spectrum in the analyzer.

The γ-ray yields are extracted from the TOF spectra plotted for events inside an energy window. The energy window is determined from the γ-ray energy (calculated from kinematics) and from the energy

calibration of the detector. The energy calibration of the detector was determined by looking at γ-rays (from radioactive sources and nuclear reactions) with energies from 0.9 MeV to 24 MeV. The channel numbers for the energy window were determined to better than 2%.

In summing the counts inside the energy window, the fractions of the counts in the first and last channel were also included, but provided a negligible contribution.

10. Target Uniformity

The beam is usually focused (as seen on a piece of quartz) to a spot 1/8" in diameter located to ±1/8" on the same position of the target. The yield at this point was checked with the yield 1/4" above and below. The target was then rotated by 90° and the three measurements were repeated. The target was found to be uniform to ±5%.

In addition, target deterioration (if any) was corrected for by normalizing the $T(d,\gamma)$ runs only to the $T(p,\gamma)$ yields taken before and after those particular measurements, to make sure that the same spot on the target was used for the $T(d,\gamma)$ runs and their corresponding $T(p,\gamma)$ calibration runs. In any case, the yields of $T(p,\gamma)$ and $T(d,\gamma)$ from the very beginning to the end of the whole experiment agree within the statistical error bars, so that the combined effects of target deterioration and different positions on the target are insignificant.

All $T(d,\gamma)$ runs were also monitored with a plastic detector and the neutron yields from $T(d,n)^4He$ provided a check on target uniformity,

beam collection, and target deterioration.

11. Spectrum Fraction

The uncertainty in the ratio $\frac{f_{T(d,\gamma)}}{f_{T(p,\gamma)}} \equiv \frac{f_d}{f_p}$ may be determined from the following considerations:

a) The spectrum fraction of a monochromatic γ-ray can be determined only to $\simeq$10% accuracy because of the uncertainty in the extrapolation of the pulse height spectrum to zero energy.

b) f_p varies by 10% from 15 MeV to 24 MeV as measured for the monochromatic γ-rays from $^{4}B(d,n\gamma)^{12}C$ and $T(p,\gamma)^{4}He$ (Table 3).

c) f_d varies by 5% over the γ-ray energy range considered, as determined from simulations of the theoretical lineshape (see Appendix 2 and Table 4).

Therefore, f_d/f_p has a systematic error on the order of 15%.

12. ^{3}He Contaminant

The tritium in the target β-decays to ^{3}He with a half-life of 12.3 years. The γ-rays from the $^{3}He(d,\gamma)^{5}Li$ reaction have energies indistinguishable, with the energy resolution in the present detector system, from those from $T(d,\gamma)^{5}He$. Moreover, the cross sections and angular distributions of the two mirror reactions are the same within experimental errors. The amount of ^{3}He in the target could be determined by measuring the high energy protons from the well-known $^{3}He(d,p)^{4}He$ reaction at the 430 keV resonance. A magnetic spectrometer could be used to select the protons of interest, but the solid state detector at the focal plane of the spectrometer would probably have to be well shielded from the intense neutron flux to prevent damage.

However, until the ^{3}He in the target can be measured, the amount of the ^{3}He will be estimated by assuming that all of it remained inside the target. This is probably an overestimate, since it is suspected that some of the ^{3}He from the tritium decay would diffuse out of the detector at an appreciable rate, especially when the target is slightly heated during bombardment. If it is assumed that the tritium gas used for the manufacturing of the target was pure (better than 99% purity is quoted by Oak Ridge), and that there are no other sources of ^{3}He contamination, then the maximum amount of ^{3}He in the target will be given by the amount of tritium that has decayed since manufacture.

By the time that most of the 90° excitation functions were being measured, approximately 8% of the tritium had decayed. Therefore, less than 8% of the yield attributed to the $T(d,\gamma)$ reaction came from the γ-rays from the ^{3}He contaminant. Since the excitation functions of the mirror reactions are similar, this contributes a systematic increase in the yield of less than 8%.

All the angles at each bombarding energy were measured at the same time (in typically less than 3 hours, including the time spent re-measuring points for consistency and pile-up checks) in order to ensure as much as possible identical experimental conditions (such as bombardment of the same point on target, with same beam energy and current.) Since the mirror reactions have similar angular distributions, then the γ-ray yields from the ^{3}He contaminant are assumed to shift the magnitude

of the angular distribution yields by much less than 11% (the fraction of tritons that had decayed by then.) Therefore, one expects that the relative yields, and thus the extracted ratio of A_2/A_0 (Figure 8) is insensitive to the amount of ^3He in the target.

13. The Extrapolation of Low Energy Background into the Energy Region of Interest

a) In the pulse height spectrum, the tail of very intense low energy γ-rays extrapolated (by eye) into the energy window contributes less than 10% to the yield.

b) At bombarding energies where the 15.1 MeV γ-rays from $^{14}N(d,\alpha\gamma)^{12}C$ are near the 0.8 E_γ^o limit, 0.9 E_γ^o was chosen as the lower boundary of the energy window. The contribution of the 15 MeV yield above 0.9 E_γ^o is then less than 1% of the $T(d,\gamma)$ yield as determined from the measured pulse height spectrum for 15 MeV γ-rays.

14. Detector Position

The axis of the crystal is lined up at 0° with the beam line to ±1/8" in a distance of 31". As the crystal is rotated the height changes by ±1/4" because of the unevenness of the floor, which causes negligible errors in angle.

The angle between the detector axis and the beam direction is known to better than 2°, to be compared with the detector angular acceptance of 15°.

The target to detector distance is known to better than 1%.

15. Anisotropy of Detection Efficiency

Asymmetry as a function of angle in the detection apparatus was tested by measuring the angular distribution of $T(p,\gamma)^4He$ which has a $\sin^2\theta$ distribution. The yields at +45°, -45° and +135° agreed within the 3% statistics.

16. Cascade Neutrons

The γ-ray transitions to the ground state of ^5He are followed by the immediate decay into an alpha particle and a low energy ($\sim$1 MeV) neutron. There is a chance that <u>both</u> the high energy γ-ray of interest and the subsequent neutron could reach the NaI detector. An event of this type would have the TOF signature of a γ-ray (the timing information is derived from the leading edge of a signal, but the signal duration is $\sim$ 1 μsec); the pulse height, however, would have contributions from the energy deposited in the crystal by both the γ-ray and the cascade neutron. Thus this kind of event would tend to distort the pulse height spectrum of the γ-rays being investigated. However, the probability of the detection of the subsequent neutron is very small because of the solid angle of the detector (less than 1%), the attenuation of the neutron in the boron-paraffin cone (more than a factor of 1000) and the detection efficiency for neutrons in NaI. Moreover, the "singles" events for these neutrons are not seen above the time-independent background in the TOF spectra. Therefore, the effect of these coincidence events is insignificant.

17. Deuterium Contaminants

At the bombarding energies used in this experiment, the deuterium beams traversed the ZrT target and were stopped in the platinum backing. Thus there might be some build-up of deuterium in the backing, giving rise to γ-rays through the $D(d,\gamma)^4He$ reaction. The γ-rays from this reaction are more energetic than those from $T(d,\gamma)$, but none were seen in the pulse height spectrum, presumably because of the small $D(d,\gamma)$ cross section.

F. Conclusions

The measured excitation function and angular distribution of the $T(d,\gamma_0)^5He$ reaction were found to be similar to those observed for the mirror reaction $^3He(d,\gamma_0)^5Li$; thus no significant violation of isospin invariance in the energy region covered by this experiment is indicated.

The broad peak in the 90° excitation function occurs in the same general excitation energy region in ^5He as a broad maximum in the cross sections for the $T(d,n)^4He$ reaction. Without the measurement of γ-ray transitions to the first excited state of ^5He, it is not possible to make the arguments for the existence of the $1/2^+$ and $5/2^+$ compound nucleus levels that were made in the case of the mirror reaction (King et al. 1972). Nevertheless, it is doubtful that, even with the measurement of the γ_1 transition rates, convincing arguments could be made regarding the highly excited states of ^5He, since there are strong reasons to suspect that there are several broad compound nucleus levels in ^5He in the energy range of the present experiment (Dodder and Hale 1975). The observed forward-backward asymmetry in the γ-ray angular distribution by itself is enough to show that both even and odd orbital angular momenta are present in the reaction, and that states with both even and odd J-values are present.

The time-of-flight techniques of the present experiment, together with careful shielding of the NaI(Tℓ) detector, have made possible a clean separation of the high energy neutrons and the gamma rays produced in the target, as well as providing a significant reduction of the time-independent background (because of the small duty cycle).

The pile-up of pulses due to a very high flux of low energy γ-rays (mainly from (d,p) and (d,n) reactions on contaminants in the target), as well as the presence of 15 MeV γ-rays attributed to the isospin-forbidden reaction $^{14}N(d,\alpha)^{12}C^*_{15.1\ MeV}$ on the ^{14}N impurity in the ZrT target, have unfortunately prevented the extraction of the γ-ray yield to the broad, first-excited state of ^5He, and have also obscured a significant portion of the γ-ray pulse height spectrum.

It is clear that greater precautions should have been taken in the manufacture of the target to avoid low Z contaminants in the target; apparently the commercial suppliers of tritium targets have not previously encountered as strict contaminant requirements as those of the present experiment. A gas cell containing highly purified tritium with gold-lined walls, and with the entrance window, the exit window and the beam dump well shielded from the detector, would certainly improve the contaminant γ-ray background situation considerably.

If it had been possible to see more of the $T(d,\gamma)$ pulse height spectrum, one would not only have been able to extract the γ_1 yields, but the counting statistics would have been improved (sum over more of the spectrum), and the cross sections would be less sensitive to the theoretical extrapolation of the pulse height to zero energy.

Careful measurements with a gas cell, moreover, would allow a determination of absolute cross sections, since the number of tritium atoms per cm^2 would be known, thus avoiding the necessity of normalizing the data to the $T(p,\gamma)$ measurements. A gas cell would also allow the two mirror reactions to be measured in the same geometry,

facilitating the isospin comparisons.

Finally, with a gas target, empty target runs, or runs with ^{4}He in the target, can be made easily to check certain sources of background.

The experimental techniques developed in this work and described here should make possible an unambiguous measurement of the cross section of the 110 keV resonance in the $T(d,\gamma)^5$He reaction excitation function, as well as the study of other capture reactions plagued by low γ-ray yields and high neutron background.

IV. THEORETICAL DESCRIPTION

A. Introduction

The energy region covered in this experiment for deuteron bombarding energies, E_d^{lab} = 2 to 12 MeV, corresponds to excitation energies (E_x) in the compound nucleus, ^{5}He, between 18 and 24 MeV. A broad enhancement in the cross section has been observed in this energy region in several reactions where ^{5}He or ^{5}Li are the compound nuclei (Figure 1).

A study (Tombrello et al. 1967) of the elastic scattering of deuterons from ^{3}He and T for bombarding energies up to 11 MeV indicates a broad resonance in the differential elastic scattering cross section corresponding to $E_x = 20 \pm 0.5$ MeV in both ^{5}He and ^{5}Li. Tombrello also examined the energy dependence of the coefficients (A_L) of the Legendre polynomial expansion of the center-of-mass angular distributions for the reactions $T(d,n)^4He$ and $^3He(d,p)^4He$. A resonance was suggested in the A_1, A_2 and A_3 coefficients for a deuteron lab energy of 5-6 MeV (E_x = 19.6 to 20.2 MeV); A_4 and A_5 also show a broad maximum but at a somewhat higher deuteron energy, E_d^{lab} = 8 to 9 MeV (E_x = 21.4 to 22.0 MeV).

The discussion in Tombrello et al. (1967) suggests that D-waves are involved in the resonance(s). It was further argued that, if the assumption is made that there is only one isolated D-wave resonance (no background) in this energy range, the only reasonable assignments for total spin and parity are $3/2^+$ or $5/2^+$. Either choice would be expected to have an appreciable channel spin $S = \frac{1}{2}$ component.

As reported earlier in this thesis, the excitation function of $T(d,\gamma)^5He_{g.s.}$ does show a broad peak, around E_d^{lab} = 7-8 MeV (E_x = 20.8 - 21.4 MeV), while in the mirror reaction, $D(^3He,\gamma)^5Li_{g.s.}$ (King et al. 1972), the peak appears at E_x = 21 MeV. In the latter experiment, the smaller neutron background and better energy resolution allowed a measurement to be made of the γ-ray transitions to the first excited state of ^{5}He as well as to the ground state. At $E_x^{^5Li}$ = 21 MeV, the 90^o cross section of the ground state transitions (γ_o) shows a broad maximum, while the cross section for the transitions to the first excited state (γ_1) goes to zero. This indicates the presence of a $5/2^+$ resonance for the following reasons: a level in the compound nucleus that decays by emission of E1 radiation to the $3/2^-$ ground level must be (by simple angular momentum addition) $5/2^+$, $3/2^+$ or $1/2^+$; a level that decays by E1 radiation to the $1/2^-$ first excited state must be $3/2^+$ or $1/2^+$. If indeed one is seeing the E1 radiation from an isolated compound nucleus level, these data indicate that the resonance has spin and parity $5/2^+$.

It is interesting to keep in mind that a resonant E1 capture through an isolated $1/2^+$ level produces an isotropic angular distribution, while resonant E1 capture through an isolated $5/2^+$ resonance gives a ratio A_2/A_o = -0.4 with the (reasonable) assumption that only channel spin 1/2 is involved in the incident channel. Furthermore, direct capture from an initial d + ^{3}He D-wave to a final bound P-wave of the same configuration has an A_2/A_o = -0.5. None of these predicted angular distributions is grossly inconsistent with the data; but

it must also be expected that the interference of several resonant and/or direct capture amplitudes, as well as the possibility of γ-ray transitions of differing multipolarity will make the picture more complicated.

In the analysis of the $T(d,\gamma)^5He$ reaction we are prevented from making some of the arguments used in the case of the mirror reaction because of the absence of data on the transitions to the first excited state. Therefore, apart from confirming the similarities in the ground-state γ-ray excitation function and angular distributions of the mirror reactions which would be expected from isospin invariance (Warburton and Weneser 1969), the main theoretical efforts of the present thesis have been focused on attempts to estimate the direct capture contribution to the radiative capture cross section. As will be discussed later, one of the quantities which could be determined from such a calculation would be the spectroscopic factor for the ground state of ^5He.

Several quite different models were considered, but only the one postulating a <u>bound</u> T + d system for the ground state of ^5He will be examined in detail here. There is no very compelling reason, however, for preferring this particular model over other possible models.

In the following sections, brief outlines will be given of the theory of direct radiative capture, and of the theory underlying the use of the optical model to describe the initial state in the reaction $T(d,\gamma)^5He$.

B. Discussion

1. Radiative Direct Capture Reactions

The calculation of the direct process in radiative capture reactions has been demonstrated (Tombrello and Parker 1963, Donnelly 1967, Rolfs 1973 and references therein) to provide a useful implement for extrapolating radiative cross sections to energy regions of astrophysical interest, and for extracting information on the structure of nuclei.

The study of the direct capture contribution to the $T(d,\gamma)^5He$ reaction was initiated in the hope that similar analysis might increase the understanding of the structure of the mass $A = 5$ nuclei.

The theoretical description of radiative direct capture reactions has been developed independently by Christy and Duck (1961) and Tombrello and Phillips (1961) to deal with radiative reactions with smooth non-resonant excitation functions and simple angular distributions. The reasonable success of the previous calculations [for example for $A = 7$ by Tombrello and Parker (1963), and for $^{16}O(p,\gamma)$ by Rolfs 1973] may be explained by the good understanding of the electromagnetic Hamiltonian, and the simplicity implied by the "extra-nuclear approximation" about to be discussed.

If the elastic scattering phase shifts of the principal ℓ-waves involved in the radiative capture are well described by scattering from a charged impenetrable sphere over a large energy range (as for the reactions considered in the previous calculations mentioned above, but not for the $T + d$ reaction), then one may suppose with some confidence that the initial wavefunctions are small over the nuclear

volume. The "extra-nuclear approximation", then, consists of neglecting all contributions to the matrix elements from the region inside the nuclear radius. Therefore, the approximation avoids the problem of nuclear forces, and will tend to be valid in regions removed from nuclear resonances, or levels in the compound nucleus.

Radiative capture reactions, whose elastic phase shifts are well represented by scattering from a charged hard sphere, are necessarily nonresonant and, since they do not follow from the formation and decay of a compound state (a two-step process), have been classified as "direct capture" reactions.

Donnelly [1967, in the treatment of the $D(p,\gamma)^3He$ reaction], Rolfs [1972, in the $^{17}O(p,\gamma)$ reaction] and Rolfs and Azuma [1974, in the $^{12}C(p,\gamma)$ reaction] have extended the applicability of the direct radiative capture formalism discussed above, by analyzing radiative capture reactions both outside and inside the region of nuclear resonances in the excitation function.

Rolfs and Azuma (1974), moreover, predicated that the resonant and nonresonant amplitudes may be determined separately, and proposed to calculate the nonresonant contribution as a direct capture process with initial wavefunctions derived from charged hard sphere scattering. Such procedure will not be attempted here.

The assumptions that went into the calculation of the direct capture in $T(d,\gamma)^5He$ will be listed later; the basic difference between this calculation and the previous ones mentioned above is the dropping of the "extra-nuclear approximation", and therefore the need

arises for determining the wavefunctions inside, as well as outside, the nuclear volume.

2. The Optical Model

Optical model potentials, determined by fitting the elastic scattering differential cross sections of the incident particles, have been used in this thesis for generating the "distorted" wavefunctions necessary in the determination of the direct radiative capture matrix elements. A great deal of research has been conducted (partly reviewed by Hodgson 1963, 1967 and 1971, and partly compiled by Perey and Perey 1972 and 1974) in trying to find an overall or global optical model potential for all nuclei, with perhaps, a smooth and easily parameterized dependence on the incident energy and on Z and A, and sometimes with systematic treatment of various effects (such as those due to spin) which will not be discussed in this thesis. The model, though, is not equally successful in all interactions and, as a word of caution, the range of applicability (discussed in more detail in the above mentioned references) will be briefly outlined.

The model appears not well suited at low excitation energies where the compound nucleus has isolated sharp levels (less than the energy resolution in the experiment); or where the "compound elastic" (the process in which the compound nucleus is first formed and then decays back into the incident channel) cross sections are significant because of the existence of only a small number of channels open to the decay of the compound nucleus. The model purports to characterize the "shape elastic" (the direct process, no intermediate state) cross

section but not the compound elastic cross section (Hodgson 1963). Generally speaking, the optical model is usually successful for reactions involving the heavier nuclei and at moderate bombarding energies (10-300 MeV) where one would suspect a large number of broad overlapping levels (diminishing the resonance effects due to single levels) in the compound nucleus, and where one would expect the compound elastic scattering to be markedly reduced by the availability of many more channels for the decay of the intermediate nucleus.

The excitation curve of the T + d reaction does reveal a broad peak (as mentioned earlier) in the region under consideration, and this enhancement may be caused by several overlapping resonances. An R-matrix analysis of the T + d and ^{3}He + d elastic reactions, and the T(d,n) and ^{3}He(d,p) reactions (Dodder and Hale 1975), as well as theoretical studies (partly summarized by King et al. 1972) using the shell model (for example, Wagner and Werntz 1971) and the cluster model (for example, Chwieroth et al. 1974, and Heiss and Hackenbroich 1971) do indicate the presence of several D-wave resonances, as well as S-wave and P-wave resonances in this region. However, the presence of only a small number of inelastic channels (the α + n, T + p + n and ^{3}He + n + n channels) may not insure the smallness of the compound elastic cross section.

At times, though, at the expense of a loss of generality, optical model fits have been found that are restricted to a particular nucleus at a particular energy, and although particular sets of data may be fitted accurately, the potentials are sometimes recognizably non-physical (Hodgson 1963).

Detailed studies of these anomalies might yield more understanding of the physical process taking place. It is beyond the scope of this thesis, however, to justify the optical model or to interpret the potentials that are used to fit the elastic scattering of $T + d$. At the very least, the optical model potentials may be considered as a convenient parameterization of the observables in the $T + d$ elastic reaction, and thus as a generator of a reasonable guess (until more detailed studies are completed) for the wavefunctions of the initial state in the direct capture calculation.

Care must be taken with such a phenomenological approach, however, since the optical potentials are not unique. More confidence would be placed on those potentials that are not inconsistent with the overall form of the potentials determined theoretically from the nucleon-nucleon interaction or from those potentials that arise from systematic parameter studies obtained by fitting the elastic data over a large range (as large as possible without sacrificing the accuracy of the fits; see Perey and Perey 1974) of energies and mass numbers around the region of interest.

C. Summary of Assumptions Underlying the Calculation

The calculation of the direct capture component (E1) in the $T(d,\gamma)^5He_{g.s.}$ reaction was carried out according to the following assumptions and procedures (many of them mentioned in the preceding section):

1) The many-nucleon problem can be approximated by a two-body problem, in which the target and projectile are treated as inert cores (point-like single particles).

2) The electromagnetic interaction Hamiltonian is well understood.

3) The radiative direct capture contribution can be described with the aid of the Hamiltonian:

$$H = H_o + H_{int}$$

where H_o contains the free electromagnetic field and the Hamiltonian of the $T + d$ system and He^5 final state, and H_{int} represents the Hamiltonian for the interaction between the particles and the electromagnetic field, leading to the emission of radiation. In the case of electric multipole radiation: H_{int} cannot change the channel spin; H_{int} is treated as a small perturbation on H_o. The perturbation approach is justified by the weakness of the electromagnetic force relative to nuclear forces as evidenced by the smallness of the cross sections for radiative capture (μbarns) when compared to the cross sections for the elastic scattering (mb to barns).

Thus, it is assumed that the use of first-order, time dependent perturbation theory (Golden Rule No. 2, Fermi 1950) is justified in the determination of the cross sections.

4) The form of the E1 operator in the long-wavelength approximation ($k_\gamma r << 1$, where k_γ is the γ-ray wave number) is proportional to the radial separation "$\vec{r}$" (Moszkowski 1968). This is the form used in the calculations described here, although for the most energetic γ-ray considered:

$$E_\gamma^{max} \simeq 25 \text{ MeV} \quad ,$$

$$k_{max} = \frac{2\pi}{\lambda} = \frac{E_\gamma^{max}}{\hbar c} \simeq 0.13 \text{ fm}^{-1} \quad ,$$

And the integrands (for the matrix element determination) were negligible (less than 1%) beyond $r_{max} \simeq 10$ fm . Therefore,

$$k_{max} r_{max} \simeq 1.3$$

The matrix elements calculated with two different versions of the "exact" radial dependence of the E1 operator (one form, used by Rolfs 1973, was presented by Donnelly 1967; the other form was derived by this author and given in Appendix 1B) differ from each other and from the matrix elements calculated with the form "$\vec{r}$" by less than 2%.

5) Correction terms, if any, to be applied in cases where there are unequal initial and final potentials, were not included.

6) In the nonresonant energy region (assumed to be free of levels in the compound nucleus) the ratio of the experimental cross section to the theoretical direct capture cross section determines the normalization of the final-state wavefunction, in the sense that the

comparison determines a value of the spectroscopic factor, $C^2S(\ell_f)$, according to the relation (Rolfs 1973):

$$\sigma_{exp} = \sum_{\ell_f} C^2S(\ell_f)\, \sigma_{theo}(\ell_f) \quad ,$$

where ℓ_f is the orbital angular momentum of the final state, and

$$C^2 = (t_p m_p t_t m_t | T_f M_f)^2$$

is the square of Clebsch-Gordan coefficient of the isospins t_p, t_t and T_f of the projectile, target and final state, respectively (see also, R. G. Thomas 1951, and Phillips and Tombrello 1960). The spectroscopic factor is considered the only adjustable parameter in the calculation; and its magnitude reflects the probability that the final nucleus will be found in the same cluster configuration as the initial state.

Since a nonresonant region is not clearly evident in the empirical $T(d,\gamma)^5He_{g.s.}$ excitation function, all the results of the direct capture calculations will be presented in this thesis with no adjustment in the overall normalization (assumed $C^2S = 1$).

7) Even though the ground state of He^5 is unbound to $\alpha + n$, it has some amplitude to be a <u>bound</u> $T + d$ system. The probability for $T + d$ clustering is given by the spectroscopic factor. An analogous assumption was made in the calculation of the direct radiative capture of $T + {}^3He$ to the first excited state of ^6Li (Ventura <u>et al</u>. 1973).

The assignment of a probability close to 1 for the ^5He ground state to look like $\alpha + n$ (Phillips and Tombrello 1960), does not

exclude an appreciable $T+d$ parentage. The reason for this is that the wavefunctions for the $T+d$ and $\alpha+n$ cluster structures in the nuclear interior are not necessarily orthogonal; since they are solutions to different Hamiltonians, they would be orthogonal only by accident (A. Winther 1975).

The spin-parity assignment for the ground state of ^{5}He is taken as $3/2^-$ (Ajzenberg-Selove and Lauritsen 1974), mainly from the observation of a $^2P_{3/2}$ resonance (channel spin, $S = \frac{1}{2}$, and orbital angular momentum, $\ell = 1$) in the scattering of neutrons by ^{4}He. This description is in agreement with a shell model picture wherein the 1s-shell is filled and the extra nucleon is in the 1p-shell ($j = 3/2$).

In the $T+d$ model of the $^5He_{g.s}$, however, a channel spin, $S = 3/2$ ($\ell = 1$, total $J = 3/2^-$) would not be ruled out; thus, in a more complete direct capture calculation, where spins are also included, the E1 operator could also connect initial $S = 3/2$ states to the ground state of ^{5}He, and spectroscopic factors could be considered for the $S = 1/2$ and $S = 3/2$ components in the final state.

8) The direct capture (single step) assumption will be made even though contributions from inside the nuclear potential are large, a situation quite different from most previous radiative direct capture studies.

Since the ground state of ^{5}He has been modeled in this calculation on the basis of a $T+d$ cluster bound very tightly ($\sim$17 MeV), the final state wavefunction has a very rapid radial decay. In addition, the enhancements in the elastic scattering show up in the matrix

elements of the direct radiative capture as increased amplitudes for the initial state inside the nuclear volume.

9) It is assumed that reliable wavefunctions to describe the initial state and final state in the direct capture may be derived from optical model potentials that have been fitted to experimental data on the elastic scattering (differential cross section measurements and all polarization studies) of the initial particles. Since the calculation of the radiative direct capture of T + d depends strongly (as will be demonstrated later) on the wavefunctions inside the nuclear surface, the model is predicated on the assumption that the more confidence one has in the optical model fits to the T + d elastic scattering data, then the more reliable will be the calculated cross sections and extracted spectroscopic factors. So far, the studies of the optical model do not verify the accuracy of the interior wavefunctions, since the calculation of the elastic scattering rates are not too sensitive to the interior contributions.

The previous radiative direct capture studies (mentioned above) have been undertaken mostly for cases in which the energy range considered was situated below the thresholds for particle channels other than the initial one; therefore, only real potentials were needed. The optical model potentials deduced from T + d elastic scattering, however, include also an imaginary part to describe the inelastic channels available.

In addition, since the particular set of potentials used in this calculation reproduced the elastic data more poorly at some angles than

at others, the total, rather than the differential, rates for direct radiative capture were determined in the hope of avoiding too great a sensitivity to the potentials in this preliminary calculation.

10) The resonances that do appear in the initial T+d state are broad and, therefore, short lived. Thus, it is assumed that the time delay is too short for any appreciable change in the cluster structure from the initial system to the final nucleus. All broad, one-channel resonances (that decay to the ground state in a one-step process) are thus inherently included in the direct capture calculation. Narrow resonances, on the other hand, may be interpreted as two-step processes: formation of the compound system and the decay of this intermediate state after a long enough delay that there has been thorough configuration mixing; that is, the compound nucleus has "forgotten how it was formed". The T+d resonance at E_d = 110 keV would be a narrow resonance from this point of view.

D. Results of the Radiative Direct Capture Calculation

The results to be presented must be considered only as preliminary because the optical model potential (from which the initial-state wavefunctions are derived) reproduces the experimental T + d elastic differential cross sections poorly (as will be demonstrated later).

1. Initial-State Potential

The potential used in this calculation was adopted from the optical model potential fitted by Lyovshin et al. (1974) to the differential cross section and the analyzing power components in the elastic scattering of the $^{3}He(d,d)\ ^{3}He$ reaction in the energy range $E^{lab}_{^{3}He}$ = 10 to 14 MeV.

In this preliminary calculation the spin dependent parts of the Lyovshin potential were neglected for simplicity; and the depth of the real part of the initial-state potential was increased from 41.625 to 45 MeV to provide slightly better agreement with the empirical T + d elastic differential cross sections measured by Tombrello et al. (1967). (The optical mode parameter space, though, was given only a cursory examination, and should be examined more carefully.)

The initial T + d wavefunctions for the radiative direct capture matrix elements were derived from an optical model potential of the following form: (Henceforth, "r" will be the radial distance between the two particles; when they appear as superscripts or subscripts, "i" and "f" refer respectively to the initial and final states; the subscripts "I" and "T" refer to the incident projectile and target particles, respectively.)

$$U_i(r) = V_{coul}(r) - V_i\, f_V^{WS}(r) + 4i\, a_W\, W \frac{df_W^{WS}(r)}{dr} \quad , \qquad (1)$$

where in the last term (at the risk of confusion) the factor

$i \equiv \sqrt{-1}$;

V_{coul} is the Coulomb potential due to a uniformly charged sphere,

$$V_{coul}(r) = \begin{cases} \frac{Z_I Z_T e^2}{2R_c}\left(3 - \frac{r^2}{R_c}\right) & \text{for } r < R_c \\ \frac{Z_I Z_T e^2}{r} & \text{for } r \geq R_c \end{cases} ;$$

and Z is the dimensionless atomic number;

$Z_I = Z_T = 1$ for the T + d case;

R is the radius parameter;

$R_c = 1.3\, A_T^{1/3}$ fermis (fm);

A is the mass number and

$A_T = 3$;

V is the real potential parameter ("volume potential");

$V_i = (45.0 + 0.124\, E_d^{lab})$ MeV;

E_d^{lab} is the laboratory deuteron energy in MeV (1 to 14 MeV);

$f^{WS}(r)$ is the Woods-Saxon form factor (Perey and Perey 1974);

$f_V^{WS}(r) = \frac{1}{1 + \exp[(r-R_V)/a_V]}$, where

$R_V = 1.75\, A_T^{1/3}$ fm ;

a is the surface diffuseness parameter;

$a_V = 0.593$ fm;

W is the strength of the imaginary, absorptive potential ("surface absorption") given by

$$W = (0.610 + 0.056\ E_d^{lab})\ \text{MeV} \ .$$

$\frac{df^{WS}(r)}{dr}$ gives the "derivative-Woods-Saxon" shape to the surface absorption;

$$\frac{df_W^{WS}}{dr} = -\frac{1}{a_W}\ \frac{\exp[(r-R_W)/A_W]}{[1 + \exp(\frac{r-R_W}{a_W})]^2} \quad , \text{ where}$$

$$R_W = (4.458 - 0.165\ E_d^{lab})A_T^{1/3}\ \text{fm} \ , \text{ and}$$

$$a_W = 0.526\ \text{fm} \ .$$

Solutions were sought to the time-independent Schrödinger wave equation for the relative motion of the two particles (the equivalent one-body problem in the center-of-mass coordinate system, Schiff 1968, eq. 18.8)

$$\nabla^2\psi(\vec{r}) + \frac{2\mu}{\hbar^2}\ [E_{CM} - U(r)]\ \psi(\vec{r}) = 0 \quad ,$$

where $U(r)$ is a potential that depends on the relative coordinates of the two particles. For the $T(d,\gamma)$ problem presented here,

$U_i(r)$ is complex and with no spin dependence;

$U_f(r)$ is real and with no spin dependence;

μ is the reduced mass;

$$\mu = \frac{M_I M_T}{M_I + M_T} \ ;$$

M is the mass of a particle;

E_{CM} is the kinetic energy associated with the relative motion;

E^i_{CM} is a positive quantity for the incident channel, given by

$$E^i_{CM} = \frac{M_T}{M_I + M_T} E_I^{lab} \quad , \quad \text{where}$$

E_I^{lab} is the kinetic energy of the incident particle in the laboratory coordinate system,

E^f_{CM} is a negative quantity for the final bound state,

$E^f_{CM} = -Q = -16.70$ MeV (Ajzenberg-Selove and Lauritsen 1974).

2. Initial-State Wavefunction

The continuum states of the deuteron-triton system can be expanded (in the center-of-mass coordinate system) in a series of spherical waves of different channel spin "S_i" and orbital angular momentum "ℓ_i" as (Donnelly 1967):

$$\psi_i^{m_i}(r) = \sum_{\ell_i} \sum_{S_i} \sqrt{4\pi(2\ell_i+1)}\ i^{\ell_i}\ e^{i\phi_{\ell_i}}\ \frac{u_{\ell_i}(k_i r)}{k_i r}\ P_{\ell_i}(\cos\theta)\ \chi^{m_i}_{S_i} \ ,$$

where the notation is that used in Appendix 1 . χ^m_S is a spin function and $u_\ell(r)$ is the radial wave function for the ℓ^{th} partial wave. The function $u_\ell(r)$ satisfies the following radial wave equation (Schiff 1968, eq. 19.1; k_i is the particle wave number):

$$\frac{d^2u_\ell}{dr^2} + \left\{\frac{2\mu}{\hbar^2}\left[E_{CM} - U(r)\right] - \frac{\ell(\ell+1)}{r^2}\right\} u_\ell = 0 \qquad (2)$$

$u_\ell(r)$ must vanish at the origin,

$$u_\ell(r=0) = 0$$

For the initial state wavefunction, $u_{\ell_i}(k_i r)$ is normalized asymptotically to unit flux (Schiff 1968, p. 116).

At a large enough radius, $r = r_{max}$, where the nuclear potential (eq. 1 without the Coulomb potential) is negligible, the wavefunction is matched to the following asymptotic form (Hodgson 1963, p. 32):

$$u_{\ell_i}(k_i r) = \frac{1}{2}\left[F_{\ell_i} + iG_{\ell_i} + S_{\ell_i}(F_{\ell_i} - iG_{\ell_i})\right] ,$$

where the radial wavefunction, $u_{\ell_i}(k_i r)$, has both real and imaginary parts. In this expression,

S_ℓ is the complex elastic scattering matrix element for the ℓ^{th} partial wave. S_ℓ depends here only on the orbital angular momentum because spin interactions have been neglected in the present calculation [Hodgson (1963) gives the corresponding treatment for spin-dependent optical model potentials when the incident particle has spin one-half or spin one];

$S_\ell = \eta_\ell e^{2i\delta_\ell}$, where

η_ℓ is the inelastic parameter (a real quantity) such that

$$0 \leq \eta_\ell \leq 1 \quad ; \quad \text{and}$$

δ_ℓ is the real nuclear elastic scattering phase shift;

F_ℓ and G_ℓ are respectively the regular and irregular normalized free Coulomb wavefunctions (Preston 1962, p. 625). F_ℓ and G_ℓ are real quantities and are functions only of the dimensionless variables ℓ , ρ and η , where $\rho = kr$;

$$k = \left(\frac{2\mu E_{CM}}{\hbar^2}\right)^{1/2}$$ is the wave number; and

$$\eta = \frac{\mu Z_I Z_T e^2}{\hbar^2 k}$$ is the Coulomb parameter

F_ℓ, G_ℓ, $\frac{dF_\ell}{d\rho}$, $\frac{dG_\ell}{d\rho}$ were determined with a computer subroutine "COUFTN" written by B. Zimmerman (Kellogg Radiation Lab.), and their values were checked against the Tubis (1957) tabulation before being used in these calculations.

The asymptotic form of $u_{\ell_i}(k_i r)$ given above is normalized to unit flux, and reduces to the incident wave, F_ℓ , when the interaction is turned off $(S_\ell = 1)$.

When only real potentials are considered (no absorption) ,

$$\eta_\ell = 1$$

and the asymptotic form becomes:

$$u_\ell = \frac{1}{2}\{F_\ell + iG_\ell + e^{2i\delta_\ell}(F_\ell - iG_\ell)\}$$

$$= e^{i\delta_\ell}\left[F_\ell\left(\frac{e^{-i\delta_\ell} + e^{i\delta_\ell}}{2}\right) + G_\ell\left(\frac{e^{+i\delta_\ell} - e^{-i\delta_\ell}}{2i}\right)\right]$$

$$= e^{i\delta_\ell}\left[F_\ell \cos\delta_\ell + G_\ell \sin\delta_\ell\right] \quad .$$

Ignoring the overall phase factor, u_ℓ may be written as a real quantity

$$u_\ell = F_\ell \cos \delta_\ell + G_\ell \sin \delta_\ell$$

This form of the asymptotic solution for real potentials agrees with the form given by Schiff (1968, p. 144) and Rolfs (1973).

3. Initial-State Elastic Scattering Cross Section

Machine calculation of the T + d elastic scattering cross section was carried out in the Berkeley CDC7600 computer with OPTMOD, a code based on the code SIGMR. SIGMR was written at the Kellogg Radiation Laboratory by G. Fox and P. R. Christensen and is a FORTRAN program for elastic scattering analyses with the optical model. This program calculates transmission coefficients,

$$T_\ell = 1 - |S_\ell|^2$$

differential elastic scattering cross sections, and absorption cross sections. This computer program is similar to one by Melkanoff et al. (1961).

OPTMOD is a version of SIGMR, revised by the author to allow for more general forms of the optical model potential, for extraction of elastic scattering phase shifts (see "S_ℓ" previously discussed), and for simpler input of parameters and easier debugging. OPTMOD was also rewritten in the form of a subroutine of the direct radiative capture code, DIRCAP (to be discussed later), with appropriate modifications to allow for extraction of properly normalized initial-state wavefunctions.

In OPTMOD, the elastic scattering wavefunctions were obtained by step-by-step numerical integration from the origin of the radial equation (2) with the potentials given in equation (1). The numerical integration procedures used in OPTMOD and DIRCAP are discussed at length in Parker (1963) for real potentials, and in Melkanoff et al. (1966).

The S-matrix elements, S_ℓ , and thus the transmission coefficients, T_ℓ , were determined by matching the logarithmic derivatives at $r_{max} = 15$ fm , of the internal wavefunction (which had been extrapolated outwards from the origin in the manner of continuation mentioned above) and the asymptotic solution.

Elastic scattering differential cross sections for the case where there are no spin interactions are given by (detailed derivations may be found in the references quoted by Hodgson 1963)

$$\frac{d\sigma}{d\Omega} = |A(\theta)|^2 \quad ,$$

Where the scattering amplitude

$$A(\theta) = f_{coul}(\theta) + \frac{1}{2ik} \sum_{\ell=0}^{\infty} (2\ell+1)(S_\ell - 1)e^{2i\sigma_\ell} P_\ell(\cos\theta) \quad .$$

θ is the center-of-mass angle;

P_ℓ is the Legendre polynomial of order ℓ ;

f_{coul} is the Coulomb scattering amplitude which is given in Hodgson (1963, eq. 2.65) and depends on k, η, σ_0 and θ ,

σ_ℓ is the Coulomb phase shift defined in Hodgson (1963, eqs. 2.51-2.52) and calculated in COUFTN, and checked against a subroutine COPS written by T. Tombrello and also against a tabulation by Sharp et al. (1966).

The transmission coefficients, T_ℓ , were determined for increasing ℓ-values until T_ℓ became negligibly small. The $T+d$ and ^3He+d elastic cross sections were calculated up to $\ell = 10$.

One of the checks of the program OPTMOD involved the calculation of the ^3He+d elastic differential cross sections for $E_d^{lab} = 10$ and 12.3 MeV with the potentials given by equation (1) except for the following changes required by the change in target:

$$V_i = (41.625 + 0.124\ E_d^{lab})\ \text{MeV}$$

$$Z_T = 2 \quad .$$

The calculated cross sections are in excellent agreement with the calculated results presented by Lyovshin et al. (1974). This agreement justifies the dropping of the spin-dependent terms in this first approximation calculation.

The $T+d$ elastic cross sections were calculated with the potentials given in equation (1) and are plotted in Figure 10, together with the data measured by Tombrello et al. (1967) and Stratton et al. (1952). Above $E_d^{lab} = 8$ MeV, the calculated $\frac{d\sigma}{d\Omega}$ are in reasonable agreement with the empirical data for the center-of-mass angles $\theta = 73.1$ and $113.4°$; at $\theta = 90°$ the calculated values are as much as 20% too high. At $\theta = 54.8°$ the calculated and measured $\frac{d\sigma}{d\Omega}$ have similar energy dependence, but above 5 MeV the calculated values are a factor of 7 too small. At 5 MeV and at the three larger angles, the agreement is very poor. However, the shapes and the calculated excitation functions at all four angles are similar to the experimental data. It would be reasonable to suppose that substantially improved fits could be

found with a more careful parameter search, using the parameters in equation (1) as starting values.

4. Final-State Wavefunctions

The final-state wavefunctions were determined on the basis of a bound P-wave T + d model for the ground state of $^{5}He(3/2^{-})$. The position of the ground state (and therefore the binding energy) was taken as the energy at which the n-α phase shift, $\delta_{3/2^{-}}$, goes through 90°.

Hodgson (1963) claims that the wavefunctions and energy levels of a bound system may be derived from potential wells which are very similar to the real part of the corresponding scattering potentials (eq. 1). Thus, the final-state potential,

$$U_f(r) = V_{coul}(r) - V_f f_V^{WS}(r) ,$$

where V_{coul} and $f_V^{WS}(r)$ have been defined previously, and

$R_c = 1.3 * 3^{1/3}$ fm ;

$R_V = 1.75 * 3^{1/3}$ fm ;

$a_V = 0.593$ fm ,

and $V_f = 61.3$ MeV.

V_f was fixed by requiring that the deuteron and triton forming the ground state of ^{5}He be bound by the experimentally determined Q-value of 16.7 MeV (Ajzenberg-Selove and Lauritsen 1974). The smallest step in the variation of V_f was .002 MeV.

The ground state wavefunction for orbital angular momentum "ℓ_f", channel spin "S_f", and total spin "J_f" can be written as (Donnelly 1967):

$$\psi_f^{m_f} = \sum_{\ell_f} \sum_{S_f} a_{\ell_f}^{S_f} \frac{u_{\ell_f}(k_f r)}{r} \sum_{\beta} (\ell_f m_f - \beta \; S_f \beta | J_f m_f) Y_{\ell_f}^{m_f - \beta}(\phi, \theta) \chi_{S_f}^{\beta}$$

where the notation is that used in Appendix 1.

The channel spin amplitudes were normalized to

$$\sum_{S_f} |a_{\ell_f}^{S_f}|^2 = 1$$

The radial wavefunction of the final state had overall unit normalization, so that

$$\int_0^{\infty} u_{\ell_f}^*(k_f r) \; u_{\ell_f}(k_f r) \; dr = 1 \quad .$$

For the ground state of ^{5}He ,

$$\ell_f = 1 \quad , \qquad S_f = \frac{1}{2} \quad ,$$

and

$$J_f = 3/2 \quad .$$

It is to be noted that there is no adjustable normalization parameter in this calculation, such as the reduced width in the final state wavefunctions used by Tombrello and Parker (1963).

The final state function, $u_{\ell_f}(k_f r)$ was calculated by step-by-step numerical integration of the radial wave equation (2) with $E_{CM} = -Q = -16.7$ MeV. The two starting values were obtained at large radii ($r_{max} = 15$ fm, where the nuclear potential is negligible), from the JWKB approximation as given by Tombrello and Parker (1963), and the values were checked with a tabulation of the Whittaker function (Abramowitz

and Stegun 1965).

5. Matrix Element of the Radiative Direct Capture Rates

The matrix elements of the electromagnetic radiation operator between continuum and bound states involved radial integrals of the form

$$R^{El}_{\ell_i \ell_f} = \int_0^\infty u^*_{\ell_f}(k_f r)\, \mathcal{O}_{El}(k_\gamma r)\, u_{\ell_i}(k_i r)\, dr \quad ,$$

where u_{ℓ_f} and u_{ℓ_i} are the bound and continuum radial wavefunctions, respectively;

k_i and k_f are the particle wave numbers;

$k_\gamma = E_\gamma/\hbar c$ where E_γ is the energy of the emitted photon,

and $\mathcal{O}_{El}(k_\gamma r)$ is the radial part of the El operator.

The results quoted here were calculated using the long-wavelength approximation (Moszkowski 1968),

$$\mathcal{O}_{El}(k_\gamma r) \xrightarrow[k_\gamma r << 1]{} r \quad ,$$

And, as mentioned previously, these results differed only slightly (less than 1%) from those using the "exact" form of the multipole operator given in Appendix 1, because the largest contributions to the integrals occurred at small values of r in the vicinity of the nuclear radius ($k_\gamma r \simeq 0.3$ for $E_\gamma = 25$ MeV).

The computer calculations were carried out in "double-precision" in the Caltech IBM 360/75 with the radiative direct capture code DIRCAP. DIRCAP is based on similar codes written by Tombrello and Parker (1963), Polchinski (1974) and Rolfs (1973), but with several modifications, among

which are provisions for handling different initial and final potentials, and for calculating real and imaginary initial-state wavefunctions derived from complex optical model potentials (based on OPTMOD as previously discussed). Like OPTMOD, DIRCAP was also revised for more efficient input of parameters, handling of program changes and debugging, and to achieve lower computing costs.

The final revised version of DIRCAP was tested by repeating several different E1 and E2 calculations carried out with the original Tombrello, Polchinski and Rolfs programs separately.

For the present $T(d,\gamma)\,^5He$ direct capture calculation, the numerical integrations (using Simpson's rule, Abramowitz and Stegun 1965) were carried out between $r = 0$ and $r = 15$ fm in steps of $\delta = 0.025$ fm; the integrand was negligible (less than a factor of 10^{-4}) at the upper limit when compared to its value near the nuclear radius ($r \simeq 4$ fm). At the resonance energy, $E_d^{lab} = 6$ MeV, the imaginary part of the matrix element was a factor of 2 larger than the real part. The contribution from the interior region ($r < R_W = 5$ fm) was approximately 90% of the total imaginary part of the matrix element, the largest value of the integrand occurring at approximately 2.5 fm.

In direct radiative capture involving particles of arbitrary spins with no spin-orbit potential, the interference terms of the various partial waves provide no contribution to the cross section integrated over the entire solid angle (Donnelly 1967); the total cross section is simply the incoherent sum over the partial cross sections. Thus,

$$\sigma(E1) = \sum_{\ell_1,\ell_f} \sigma(E1, \ell_i \rightarrow \ell_f) .$$

From Appendix 1A, the total cross section for E1 direct capture from a continuum state with orbital angular momentum, ℓ_i , to a bound state with orbital angular momentum, ℓ_f , and total angular momentum (orbital plus spin), J_f , is given by

$$\sigma(E1,\ \ell_i \rightarrow \ell_f) = N\mu^{3/2}\left(\frac{Z_I}{M_I} - \frac{Z_T}{M_T}\right)^2 \frac{E_\gamma^3}{(E_{CM}^i)^{3/2}}$$

$$\times \quad \frac{(2J_f+1)(2\ell_i+1)}{(2s_I+1)(2s_T+1)(2\ell_f+1)} (\ell_i 010|\ell_f 0)^2 \ (R^{E1}_{\ell_i\ell_f})^2 \quad ,$$

where, as previously defined, $R^{E1}_{\ell_i\ell_f}$, μ , E^i_{CM} , E_γ , Z and M are the radial integral, the reduced mass, the kinetic energy of relative motion, the γ-ray energy in the center-of-mass coordinate system, the atomic number and the mass, respectively.

s is the intrinsic particle spin, and

$(\ell_i 010|\ell_f 0)$ is a Clebsch-Gordan coefficient.

$$N = \frac{8\pi}{3\sqrt{2}} \alpha \frac{1}{\hbar c} \quad ;$$

$$\alpha = \frac{e^2}{\hbar c} \simeq \frac{1}{137}$$ is the dimensionless fine structure constant,

and $\hbar c \simeq 197$ MeV-fm.

Since $\sigma(E1)$ has the dimensions of length, the wavefunctions $u_{\ell_i}(kr)$ are dimensionless and u_{ℓ_f} have dimensions of $(1/\text{length})^{1/2}$. R^{2^i} has the dimensions of $(\text{length})^3$. To get $\sigma(E1)$ in barns, when E_γ and E^i_{CM} are in MeV, and the M's are in amu (1 amu = 931.478 MeV),

$$N \simeq \frac{8}{3\sqrt{2}} \frac{1}{137} \frac{1}{197} \frac{1}{\sqrt{931.478}} \times 10^4$$

$$\simeq 0.0718 .$$

The factor of 10^4 is for converting from $fm^2 = 10^{-26} cm^2$ to $\mu b = 10^{-30} cm^2$.

The cross sections for radiative direct capture of T + d were calculated for transitions to a single final orbital angular momentum $\ell_f = 1$ ($J^\pi = 3/2^-$ for $^5He_{g.s.}$).

Angular momentum and parity conservation for the emission of E1 radiation (angular momentum and parity quantum numbers = 1^-) allow decay only from two initial partial waves, $\ell_i = 0$ and 2.

The E1 direct capture total cross section to the ground state is plotted in Figure 11, along with the partial cross sections for S and D waves. The transitions appear to proceed chiefly by capture from the D-waves, which resonate between 7 and 8 MeV. The calculated E1 capture cross section peaks around 6 MeV while the experimentally determined cross sections resonate between 7.5 and 8 MeV. The maximum of the calculated cross section is only about one-half of the maximum in the experimental cross section curve. The calculated cross section above and below the broad peak fall off somewhat faster than the empirical data; however, the shapes of the calculated and measured excitation functions are similar.

6. Sensitivity to the Parameters in the E1 Calculation

The sensitivity of the E1 cross section as given by the bound-final-state model has been investigated for some of the various parameters in the calculation. The results are tabulated in Table 6 . [The parameter dX/dE gives the linear dependence of the potential on E_d^{lab} as given in eq. (1).]

7. M1 and E2 Transitions

The M1 (orbital) direct capture was calculated for $\ell_i = 1$ only, since the operator cannot change the orbital angular momentum. The calculated maximum ratio of the rates, M1/E1, was less than 5%.

The E2 direct capture rate was determined for $\ell_i = 1$, 3, and 5. The rates from P and H waves were comparable, but the main E2 contribution came from the F-wave capture. Even so, the calculated maximum E2/E1 ratio was less than 0.3%.

It is interesting to note that the interference of the various multipole emissions appears in the angular distribution as terms that depend on odd-ℓ Legendre polynomals (Donnelly 1967 gives useful formulae for several types of interference terms). Thus, even if the direct capture rates from M1 and E2 transitions make a negligible contribution to the total radiative direct capture cross section, the interference of these processes may help explain the small forward-backward asymmetry found in the experimental $T(d,\gamma)\,{}^{5}He_{g.s.}$ angular distribution.

E. Conclusions

With the potential parameters fixed entirely by fitting the experimental T + d elastic scattering cross sections, and by the experimentally known "binding energy" (Q-value) of the ground state of ^{5}He, fair agreement with the shape of the experimental radiative capture cross section curve is obtained, although there is a discrepancy of approximately a factor of 2 in the magnitude of the total cross sections.

More accurate optical model fits to the elastic scattering might improve the agreement in shape and magnitude.

It is possible, however, that the broad peak in the excitation function should be interpreted as resonant radiative capture proceeding through several broad levels in the compound nucleus, and that the empirically observed asymmetry may arise from the interference between resonances of opposite parity. The analysis of Dodder and Hale (1975) indicates the presence of several D and S waves in the region of the cross section enhancement, as well as P and F levels at higher energies.

It is, therefore, difficult to assess the significance of the differences between the results obtained using this direct capture model and the empirical data.

It would certainly be premature at this time to attempt the extraction of a spectroscopic factor for the ^{5}He ground state. This may become possible when a more complete analysis of the elastic scattering of deuterium on tritium becomes available.

APPENDIX 1A

RADIATIVE DIRECT CAPTURE CROSS SECTION TO BOUND STATES

The theoretical expressions for the radiative direct capture cross sections may be found in Parker (1963), Donnelly (1967) and Rolfs (1973). The derivations of the multipole operators (except the "exact" form) came from Weidenmüller (1962) and Moszkowski (1968). Therefore, only a brief outline will follow. Spinless interactions are assumed, along with other assumptions enumerated on page 49.

The radiative direct capture reaction may be described by the Hamiltonian

$$H = H_{(\text{system})} + H_{(\text{photons})} + H_{\text{int}}$$

where $H_{(\text{system})}$ contains the kinetic energy of the particles plus the potential energy of their nuclear and Coulomb interactions;

$H_{(\text{photons})}$ contains the energy of the free electromagnetic field;

and where the interaction Hamiltonian for a photon with the nuclear system is

$$H_{\text{int}} = -\frac{1}{c}\int d^3x\, \vec{j} \cdot \vec{A}$$

where $\vec{j}$ is the nuclear-charge current vector; and

$\vec{A}$ is the vector potential of the photon field.

For a system of point particles,

$$j(\vec{r}) = \sum_i \frac{q_i}{M_i}\, \vec{p}_i\, \delta(\vec{r}-\vec{r}_i)$$

Therefore,

$$H_{int} = -\frac{1}{c}\sum_i \frac{q_i}{M_i}\vec{p}_i \cdot \vec{A}$$

where the summation runs over all the particles with charge q_i, mass M_i.

Considering the case where a photon of polarization P is created, and normalizing the total energy to $\hbar\omega$ in the volume V,

$$(\vec{A}^P(\vec{r},t))^* = -i\left(\frac{2\pi\hbar c^2}{V\omega}\right)^{1/2} \hat{\varepsilon}_P^* \, e^{-i\vec{k}_\gamma\cdot\vec{r}} \quad ,$$

where $\hat{\varepsilon}_p$ is a spherical unit vector in the direction P and $\vec{k}_\gamma$ is the photon wave vector. Expanding in multipoles, and considering only electric multipole operators:

$$\vec{A}^{*P} = -i\left(\frac{2\pi\hbar c^2}{V\omega}\right)^{1/2} \sum_{L,M} \sqrt{2\pi(2L+1)}\,(-i)^{L+1}\, {}^P\mathcal{D}_L^{*M,P}(\phi_\gamma,\theta_\gamma,0)\vec{A}_L^{*M}(e) \tag{1}$$

where $\mathcal{D}_L^{*M,P}$ is an element of the rotation matrix, and

$\omega = k_\gamma c$.

Simplifying further to the case of the E1 operator in the long-wavelength approximation, considering two particles and expanding in the center-of-mass system (Appendix 1B),

$$H_{int}^P = icek_\gamma\left(\frac{2\pi\hbar}{\omega V}\right)^{1/2} \sum_M (-i)\left(\frac{4\pi}{3}\right)^{1/2} {}^P\mathcal{D}_1^{*M,P}\left(\frac{M_I M_T}{M_I+M_T}\right)\left(\frac{Z_I}{M_I}-\frac{Z_T}{M_T}\right) r\, Y_1^{*M}(\theta,\phi)$$

where r, θ and ϕ are the relative coordinates of the two particles.

From Fermi's golden rule, the differential cross section in the center-of-mass coordinate system can be written as

$$\frac{d\sigma(\theta)}{d\Omega} = \frac{2\pi}{\hbar v_i} \frac{d\hat{N}}{dE\ d\Omega} \frac{1}{(2s_I+1)(2s_T+1)} \sum_{m_i,m_f,P} |\langle \psi_f^{m_f} | H_{int}^{P} | \psi_i^{m_i} \rangle|^2 \quad ,$$

where v_i is the relative velocity of the initial channel;

s_I and s_T are the spins of the incident and target particles, respectively; and

$\psi_i^{m_i}$ and $\psi_f^{m_f}$ are the wave functions of the initial state and final state with magnetic quantum numbers m_i and m_f, respectively.

The energy density of final states (recoil nucleus + photon) can be well approximated using the one-particle phase space of the photon:

$$\frac{dN}{dE} = \frac{V}{(2\pi\hbar)^3} \frac{d^3 \vec{p}_\gamma}{dE_\gamma}$$

where $$p_\gamma = \frac{E_\gamma}{c} = \frac{\hbar\omega}{c} \quad .$$

Therefore,

$$\frac{dN}{dE} = \frac{p_\gamma^2 \frac{dp_\gamma}{dE_\gamma} d\Omega V}{(2\pi\hbar)^3} = \frac{V\omega^2 d\Omega}{8\pi^3 \hbar c^3}$$

The initial-state wavefunction can written as

$$\psi_i^{m_i} = \sum_{\ell_i} \sum_{S_i} \sqrt{4\pi(2\ell_i+1)}\ i^{\ell_i}\ e^{i\phi_{\ell_i}}\ \frac{u_{\ell_i}}{k_i r}\ Y_{\ell_i}^{o}(\theta,\phi)\ \chi_{S_i}^{m_i}$$

where $\phi_{\ell_i}^{S_i} = \sigma_{\ell_i} - \sigma_o + \delta_{\ell_i}$;

σ_ℓ is the Coulomb phase shift;

δ_ℓ is the nuclear phase shift;

k_i is the particle wavenumber;

$\chi_{S_i}^{m_i}$ is the spin function for the channel spin S_i ;

u_{ℓ_i} is the radial wavefunction for the initial state, normalized asymptotically to unit flux.

The final bound-state wavefunction can be written as

$$\psi_f^{m_f} = \sum_{\ell_f} \sum_{S_f} a^{S_f} \frac{u_{\ell_f}}{r} \sum_{\beta} (\ell_f S_f m_f - \beta \, \beta | S_f m_f) \, Y_{\ell_f}^{m_f - \beta}(\theta,\phi) \, \chi_{S_f}^{\beta}$$

where the a^{S_f} is the channel spin amplitude, normalized to

$$\sum_{S_f} |a^{S_f}|^2 = 1$$

and u_{ℓ_f} is the radial wavefunction with the normalization condition

$$\int_0^\infty |u_{\ell_f}|^2 \, dr = 1 \, .$$

The total cross section for E1 direct capture is then determined by carrying out the integrals over the photon and particle angular variables; the incoherent sum over the channel spin S_f , and the sums over the photon polarization and the magnetic quantum numbers. This procedure has been written out in detail by Rolfs (1973, Appendix A.1); therefore

only the result will be quoted:

$$\sigma(E1,\ \ell_i \to \ell_f) = \frac{8\pi}{3\sqrt{2}} \left(\frac{e^2}{\hbar c}\right) \frac{1}{\hbar c} \left(\frac{M_I\ M_T}{M_I + M_T}\right)^{3/2}$$

$$\times \left(\frac{Z_I}{M_I} - \frac{Z_T}{M_T}\right)^2 \frac{E_\gamma^3}{(E_{CM}^i)^{3/2}} \frac{(2J_f+1)(2\ell_i+1)}{(2s_I+1)(2s_T+1)(2\ell_f+1)}$$

$$\times (\ell_i 010 | \ell_f 0)^2 \ (R^{E1}_{\ell_i \ell_f})^2$$

where E^i_{CM} is the kinetic energy of relative motion;

J_f is the total angular momentum of the final state; and

$$R^{E1}_{\ell_i \ell_f} = \int_0^\infty \frac{u_{\ell_f}}{r}\, r\, \frac{u_{\ell_i}}{r}\ r^2\, dr \quad .$$

APPENDIX 1B

"EXACT" FORM OF THE ELECTRIC MULTIPOLE OPERATOR

The electric operator in equation (1) of Appendix 1A may be written (Weidenmüller 1962) as

$$\vec{A}^{M}_{L}(e) = \frac{-i}{\sqrt{L(L+1)}} \frac{1}{k_\gamma} \text{curl}\{\vec{L}\, u_{LM}\} \quad ,$$

$$u_{LM} = j_L(k_\gamma r)\, Y^M_L(\theta_\gamma, \phi_\gamma) \quad ,$$

where j_L is a spherical Bessel function;

Y^M_L is the spherical harmonic and depends on the center-of-mass angles of the photon;

and $\nabla^2 u_{LM} + k^2_\gamma u_{LM} = 0$.

The angular momentum operator is

$$\vec{L} = -i\, \vec{r} \times \vec{\nabla}$$

Therefore,

$$\vec{A}^{M}_{L}(e) = \frac{(-i)(-i)}{k_\gamma \sqrt{L(L+1)}} \vec{\nabla} \times (\vec{r} \times \vec{\nabla}) u_{LM}$$

$$= \frac{-1}{k_\gamma \sqrt{L(L+1)}} [\vec{r}\nabla^2 - \vec{\nabla}(1 + \vec{r} \cdot \vec{\nabla}]u_{LM} \qquad \text{(identity)}$$

$$= \frac{1}{k_\gamma \sqrt{L(L+1)}} [k^2_\gamma \vec{r} + \vec{\nabla}(1 + r \frac{\partial}{\partial r})]u_{LM} \qquad (1)$$

In evaluating the matrix element

$$\langle f|\vec{p} \cdot \vec{A}^{M*}_{L}(e)|i\rangle \qquad (2)$$

where $\vec{p} = \frac{\hbar}{i}\vec{\nabla}$ acts on everything to the right (as indicated by the arrows), the first term (from equation 1) depends on

$$k_\gamma^2 \langle f|\vec{p} \cdot \vec{r}\, u^*_{LM}|i\rangle$$

$$= k_\gamma^2[\langle f|\frac{\hbar}{i}\vec{\nabla} \cdot (\vec{r}\, u^*_{LM})|i\rangle$$

$$+ \langle f|u^*_{LM}\, \vec{r} \cdot \vec{p}|i\rangle]$$

$$= \frac{\hbar k_\gamma^2}{i}[\langle f|r(\frac{\partial u^*_{LM}}{\partial r})|i\rangle + 3\langle f|u^*_{LM}|i\rangle$$

$$+ \langle f|u^*_{LM}\, r\, \frac{\partial}{\partial r}|i\rangle]$$

since $\vec{\nabla} \cdot (\vec{r}\, u^*_{LM}) = \vec{r} \cdot \vec{\nabla}\, u^*_{LM} + u^*_{LM}\, \vec{\nabla} \cdot \vec{r}$

and $\vec{\nabla} \cdot \vec{r} = 3$.

This term in the matrix element (eq. 2) agrees with the expression given by Brennan and Sacks (1952) but will be dropped because it is smaller compared to the second term (to be evaluated later) by the factor Mc^2/E_γ = the mass of the particle divided by the photon energy .

In evaluating the second term in the matrix element (eq. 2) arising from the second term in equation (1), the following relationship may be proved in a manner similar (but more complicated) to the one used above:

$$\langle f|\vec{p} \cdot \vec{\text{grad}}\, U|i\rangle = \frac{M}{-i\hbar}\langle f|\frac{p^2}{2M}U - U\frac{p^2}{2M}|i\rangle$$

$$+ \frac{\hbar}{2i}\langle f|\nabla^2 U|i\rangle \qquad (3)$$

where $U = (1 + r\frac{\partial}{\partial r})\, u^*_{LM}$.

If V_i and V_f are the initial and final potentials of the nuclear system with eigenenergies E_i and E_f respectively, then

$$(\frac{p^2}{2M} + V_i)|i\rangle = E_i|i\rangle$$

$$(\frac{p^2}{2M} + V_f)|f\rangle = E_f|f\rangle$$

Adding and subtracting $(V_f - V_i)$ in equation (3)

$$\langle f|\vec{p} \cdot \vec{\text{grad}}\, U|i\rangle = \frac{iM}{\hbar}\langle f|(\frac{p^2}{2M} + V_f)U - U(\frac{p^2}{2M} + V_i)|i\rangle$$

$$- \frac{iM}{\hbar}\langle f|V_f U - UV_i|i\rangle - \frac{i\hbar}{2}\langle f|\nabla^2 U|i\rangle$$

Therefore, the second term in the matrix element (eq. 2) may be calculated using the following relationship:

$$\langle f|\vec{p} \cdot \vec{\text{grad}}\, U|i\rangle = \frac{iM}{\hbar}(E_f - E_i)\langle f|U|i\rangle - \frac{iM}{\hbar}\langle f|(V_f - V_i)U|i\rangle$$

$$- \frac{i\hbar}{2}\langle f|\nabla^2 U|i\rangle \qquad (4)$$

The last term in eq. (4) is small and again will be dropped. The correction term for unequal initial and final potentials will also be dropped for convenience. Therefore, the matrix element becomes:

$$\langle f|\vec{p}_j \cdot \vec{A}_L^{M*}(e)|i\rangle$$

$$= \frac{-iM\omega}{k_\gamma\sqrt{L(L+1)}} \langle f|u_{LM}^* + r\frac{\partial u_{LM}^*}{\partial r}|i\rangle$$

$$= \frac{-iMc}{\sqrt{L(L+1)}} \langle f|Y_{LM}^*(j_L + \rho\frac{dj_L}{d\rho})|i\rangle$$

where $\rho = k_\gamma r$;

$\omega = \frac{-(E_f-E_i)}{\hbar}$; and

$$j_L + \rho\frac{dj_L}{d\rho} = \rho j_{L-1} - Lj_L \ .$$

For the E1 operator, $L = 1$, and this expression becomes

$$\rho j_0 - j_1 = \frac{1}{\rho^2}[(\rho^2-1)\sin\rho + 1\rho\cos\rho]$$

which is similar to expression given (without proof) by Donnelly (1967), except that he shows a "2" where the above has a "1". Doing the sum $\sum \frac{q_j}{M_j}\vec{p}_j\vec{A}^*(e)$ over all particles ($q_j = eZ_j$; $j = 1,2$), and neglecting the motion of the center-of-mass system (Radomski 1975), the radial part of the electric multipole operator is given by:

$$\sigma'_{(EL)} = Z_1[\alpha r\, j_{L-1}(\alpha r) - L j_L(\alpha r)]$$

$$+ Z_2[-\beta r\, j_{L-1}(-\beta r) - L j_L(-\beta r)] \qquad (4)$$

where

$$\alpha = \frac{M_2 k_\gamma}{M_1+M_2} \quad ; \qquad \beta = \frac{M_1 k_\gamma}{M_1+M_2} \quad .$$

In the long-wavelength approximation

$$\sigma'_{(EL)} \xrightarrow[k_\gamma r << 1]{} \frac{L+1}{(2L+1)!!}\,[Z_1(\alpha r)^L + Z_2(-\beta r)^L]$$

and for the E1 operator (L = 1):

$$\sigma'_{(E1)} \longrightarrow \frac{2}{3}\left(\frac{M_1 M_2}{M_1+M_2}\right) k_\gamma \left(\frac{Z_1}{M_1} - \frac{Z_2}{M_2}\right) r$$

This form of the operator agrees with Moszkowski (1968).

APPENDIX 2

Simulation of the $T(d,\gamma)^5He$ Pulse Height Spectrum

To simulate the pulse height spectrum of gamma rays to the unbound ground state and first excited state of ^5He, it was necessary to assume theoretical lineshapes for the two decays. A convenient representation of the spectral shapes was used which was analogous to one in the analysis of the mirror reaction (King et al. 1972, and references therein):

$$G(E_\gamma) = E_\gamma^3 \left[a_0 \frac{\sin^2\beta_0}{P} + a_1 \frac{\sin^2\beta_1}{P}\right]$$

where $G(E_\gamma)$ is the (theoretical) gamma intensity at energy E_γ ;

β is the resonant $n+\alpha$ phase shift ;

P is the Breit-Wigner penetrability for $\ell = 1$ (Preston 1962, p. 517) ;

a is the transition strength ;

subscript 0 is the transition to $3/2^-$ ground state ; and

subscript 1 is the transition to $1/2^-$ first excited state.

The factor E_γ^3 arises from an assumption of E1 transitions. The resonant phase shifts were computed from literature values of the $n + \alpha$ scattering phase shifts (Arndt and Roper 1973), assuming that the hard sphere phase shift corresponds to a radius of 2.5 fm. The resonant phase shift β_ℓ is defined as follows (Lane and Thomas, pp. 269-281):

$$\beta_\ell = \delta_\ell + \Phi_\ell - \omega_\ell$$

where δ_ℓ is the total phase shift ;

$-\Phi_\ell$ is the hard sphere phase shift ; and

ω_ℓ is the Coulomb phase shift = 0 for neutrons.

The actual photon spectrum G_E and the pulse height spectrum produced by the detector N_K are related by:

$$N_K = \sum_E \varepsilon_E \, G_E \, A_{E,K} \quad ; \quad G_E \equiv G(E_\gamma)$$

where ε_E is the detection efficiency of NaI crystal and boron-paraffin attenuation at energy E (see page 22); and

$A_{E,K}$ is the probability that photon of energy E is assigned a channel K by the multichannel analyzer connected to the detector.

The detector response function for a monoenergetic γ-ray of energy E was parameterized as follows (King et al. and references therein):

$$A_{E,K} = \alpha_0 + \alpha_1 \exp[\alpha_2(K-E)] \quad , \quad K < E \quad ,$$

$$A_{E,K} = \alpha_3 \exp[-\alpha_4(K-E)^2] \quad , \quad K \geq E \quad ,$$

$$\alpha_3 = \alpha_0 + \alpha_1$$

where α_0, α_1, α_2, α_3, α_4 are empirical, energy-dependent parameters. The parameters used here were determined by a nonlinear, least-squares fit to monoenergetic gamma spectra from the reactions $T(d,\gamma)^4He$ and $^{11}B(d,n\gamma_{15.1})^{12}C$, the standard spectra were accumulated at identical experimental conditions (such as target-to-detector distance, attenuator

and collimation) as the T(d,γ) reaction. Figure 4 shows a typical T(p,γ) lineshape and the fit using the analytic form above. A horizontal extrapolation of the lineshape to zero energy was assumed. The exact form of the lineshape in the low pulse height region is not known, and this introduces an uncertainty in the absolute cross section of about 10%. The lineshape fitting was carried out with the computer code NAIPK which is based on the program CURFIT given by Bevington (1969, p. 237).

REFERENCES

A. Abramowitz and I. Stegun 1965, Handbook of Mathematical Functions (Dover Pub., New York).

F. Ajzenberg-Selove and T. Lauritsen 1974, Nuc. Phys. A227, 1.

R. A. Arndt and L. D. Roper 1973, Nuc. Phys. A209, 447.

P. R. Bevington 1969, Data Reduction and Error Analysis for the Physical Sciences (McGraw-Hill, New York).

V. M. Bezotosnyi, V. A. Zhmailo, L. M. Surov and M. S. Shvetsov 1970, Soviet J. Nuc. Phys. 10, 127.

J. M. Blatt and L. C. Biedenharn 1952, Rev. Mod. Phys. 24, 258.

J. G. Brennan and R. G. Sachs 1952, Phys. Rev. 88, 824.

C. P. Browne, W. A. Schier and I. F. Wright 1965, Nuc. Phys. 66, 49.

W. Buss, H. Wäffler and B. Ziegler 1963, Phys. Lett. 4, 198.

R. F. Christy and I. Duck 1961, Nucl. Phys. 24, 89.

F. S. Chwieroth, Y. C. Tang and D. R. Thompson 1974, Phys. Rev. C4, 56.

J. H. Coon and R. W. Davis 1959, Bull. Am. Phys. Soc. 4, 365.

F. S. Dietrich 1964, Ph.D. Thesis, California Institute of Technology.

D. C. Dodder and G. M. Hale 1975, Private communication.

T. W. Donnelly 1967, Ph.D. Thesis, University of British Columbia.

P. L. Dyer 1973, Ph.D. Thesis, California Institute of Technology.

A. Fässler 1965, Nuc. Phys. 65, 329.

A. J. Ferguson 1965, Angular Correlation Methods in Gamma-Ray Spectroscopy (North-Holland, Amsterdam).

E. Fermi 1950, Nuclear Physics (U. of Chicago Press, Chicago).

G. Fox and P. R. Christensen 1975, Private communication.

G. W. Grodstein 1957, NBS Circular 583.

P. Heiss and H. Hackenbroich 1971, Nuc. Phys. A162, 530.

P. E. Hodgson 1963, The Optical Model of Elastic Scattering (Oxford University Press, Amen House, London EC4).

P. E. Hodgson 1967, Ann. Rev. Nuc. Science 17, 1.

P. E. Hodgson 1971, Nuclear Reactions and Nuclear Structure (Clarendon Press, Oxford).

B. Hoop Jr. and H. Barschall 1966, Nuc. Phys. 83, 65.

H. T. King, W. E. Meyerhof and R. G. Hirko 1972, Nuc. Phys. A178, 337.

A. Kosiara and H. B. Willard 1970, Phys. Lett. 32B, 99.

A. M. Lane and R. G. Thomas 1958, Rev. Mod. Phys. 30, 257.

J. D. Larson 1965, Ph.D. Thesis, California Institute of Technology.

N. H. Lazar, R. C. Davis and P. R. Bell 1956, Nucleonics 14, 52.

E. B. Lyovshin et al. 1974, Phys. Lett. 52B, 392.

J. B. Marion and J. L. Fowler 1960, Fast Neutron Physics, Part I (Interscience, New York).

J. B. Marion and F. C. Young 1968, Nuclear Reaction Analysis (North-Holland, Amsterdam).

M. A. Melkanoff, D. S. Saxon, J. S. Nodvik and D. G. Cantor 1961, A FORTRAN Program for Elastic Scattering Analyses with the Nuclear Optical Model (University of California Press, Berkeley and Los Angeles).

M. A. Melkanoff, T. Sawada and J. Raynal 1966 in Methods in Computational Physics, Vol. 6, Nuclear Physics, ed. by B. Alder, S. Fernbach, and M. Rotenberg (Academic Press).

W. E. Meyerhof, M. Suffert and W. Feldman 1970, Nuc. Phys. A148, 211.

S. A. Moszkowski 1968, Alpha, Beta and Gamma-Ray Spectroscopy, ed. K. Siegbahn (North-Holland, Amsterdam), p. 863 ff.

P.D.M. Parker 1963, Ph.D. Thesis, California Institute of Technology.

J. D. Pearson 1963, Ph.D. Thesis, California Institute of Technology.

C. M. Perey and F. G. Perey 1972, Nuclear Data Tables 10, 539.

C. M. Perey and F. G. Perey 1974, Atomic Data and Nuclear Data Tables 13, 293.

J. E. Perry, Jr. and S. J. Bame 1955, Phys. Rev. 99, 1368.

J. Polchinski 1974, Private communication.

J. Polchinski 1975, Private communication.

M. A. Preston 1962, Physics of the Nucleus (Addison-Wesley, Massachusetts)

M. Radomski 1975, Private communication.

C. Rolfs 1973, Nuc. Phys. A217, 29.

C. Rolfs and R. E. Azuma 1974, Nuc. Phys. A227, 291.

M. E. Rose 1953, Phys. Rev. 91, 610.

G. Satchler et al. 1968, Nuc. Phys. A112, 1.

G. A. Sawyer and L. C. Burkhardt 1955, Phys. Rev. 98, 1305.

L. I. Schiff 1968, Quantum Mechanics, 3rd Edition (McGraw-Hill, New York).

W. T. Sharp, H. E. Gove and E. B. Paul 1966, AECL-268, Chalk River, Ontario.

W. F. Stratton et al.1952, Phys. Rev. 88, 257.

R. G. Thomas 1951, Ph.D. Thesis, California Institute of Technology.

T. A. Tombrello and G. C. Phillips 1961, Phys. Rev. 122, 224.

T. A. Tombrello and P. D. Parker 1963, Phys. Rev. 131, 2582.

T. A. Tombrello, R. J. Spiger and A. D. Bacher 1967, Phys. Rev. 154, 935.

A. Tubis 1957, LASL Report No. LA-2150.

E. Ventura, J. R. Calarco, W. E. Meyerhof and A. M. Young 1973, Phys. Lett. 46B, 364.

R. F. Wagner and C. Werntz 1971, Phys. Rev. C4, 1.

E. K. Warburton and J. Weneser 1969, The Role of Isospin in Electromagnetic Transitions in Isospin in Nuclear Physics , ed. D. H. Wilkinson (North-Holland, Amsterdam).

H. A. Weidenmüller 1962, Theoretical Nuclear Physics (unpublished lecture notes).

W.S.C. Williams 1964, High Energy and Nuclear Physics Data Handbook (Rutherford Laboratory, Chilton).

A. Winther 1975, Private communication.

C. D. Zerby and H. S. Moran 1961, Nuc. Instr. & Meth. 14, 115.

TABLE 1

Detection Efficiency for 8"x5" NaI(Tℓ) at 31" from Target
(see text, p. 21)

Absorbing medium: paraffin + B_2O_3 cone (29")

glass wall - 3/16"

1/16" lead

Steel housing and Al_2O_3 around crystal

$$d\Omega/4\pi = 0.4 \times 10^{-2}$$

$$J_n = \frac{1}{2\pi} \int_{\text{crystal}} P_n(\cos\theta)\ \underbrace{e^{-\mu_1 \ell_1}}_{\substack{\text{attenuation} \\ \text{in absorbing} \\ \text{medium}}}\ \underbrace{(1 - e^{-\mu_2 \ell_2})}_{\substack{\text{detection} \\ \text{in NaI}}}\ d\Omega$$

attenuation factors $Q_n = J_n/J_o$;

$$W^{CM}_{obs}(\theta_{CM}) = \sum_n A_n Q_n P_n(\cos\theta_{CM})$$

	Detection Efficiency			$e^{-\mu_1 x_1}$	$1 - e^{-\mu_2 x_2}$
E_γ	$\varepsilon \equiv J_o/2$	Q_1	Q_2	attenuation in cone	detection in NaI
19.0	0.8×10^{-3}	.996	.989	0.27	0.86
24.9	0.9×10^{-3}	.996	.989	0.29	0.88

TABLE 2

Attenuation of 19.5 MeV γ-Rays in the Material between Target and NaI Detector - See text, p. 22.

MATERIAL	LENGTH	TRANSMISSION ($e^{-\mu x}$)
paraffin + B_2O_3	29"	0.31
glass	3/16"	0.98
lead sheet	1/16"	0.89
stainless steel housing of crystal	0.019"	0.99
Al_2O_3 reflector of the crystal	1/16" (67 mg/cm^2)	0.99
target and target backing	3 mg/cm^2 Zr 10 mil Pt 1/8" Cu	0.90*

*at $\theta = 0°$ runs only.

TABLE 3

Measurements of the Spectrum Fraction for Monochromatic γ-Rays. See text, p. 22.

E_γ (MeV)	Spectrum Fraction (0.8 E_γ^o to 1.1 E_γ^o)
24.22	0.42
23.1	0.40
22.74	0.40
21.99	0.42
20.88	0.39
15.11	0.38

TABLE 4

Simulation of Pulse Height Spectrum for $T(d,\gamma)\ ^5He$

See text, p. 22 and Appendix 2.

		Only Transitions to Ground State		Equal Amplitudes for Transitions to Ground State and First Excited State	
E_d^{lab} (MeV)	E_γ (MeV)	f (spectrum) fraction	FWHM	f	FWHM
2	17.8	0.40	48%	0.38	74%
6	20.2	0.38	44%	0.37	71%
12	23.7	0.38	41%	0.39	66%

TABLE 5

Results of Fits to Angular Distribution

See text, p. 26.

E_d^{lab} (MeV)	$E(He^5)$ (MeV)	Fit with $A_o+A_2P_2$	Fit with $A_o+A_1P_1+A_2P_2$	
		A_2/A_o	A_2/A_o	A_1/A_o
4	19.0	-.03 ± .07	.02 ± .10	-.07 ± .10
8	21.4	-.20 ± .07	-.13 ± .08	-.10 ± .08
10	22.6	-.30 ± .07	-.26 ± .10	-.05 ± .10
12	23.8	-.44 ± .06	-.34 ± .06	-.11 ± .06

Table 6

Parameter Sensitivity of Total Direct Capture Calculation of $T(d,\gamma_{E1})^5He_{g.s.}$
(See text, p. 69)

Parameter	Original value	Variation in Parameter	Maximum Variation in Calculated Cross Section
limit on radial integration and mesh size:			
r_{max}	15 fm	20 fm	< 1%
δ_r	0.025 fm	0.010 fm	< 1%
initial-state potential parameters [in eq. (1), p. 56]:			
R_c	$1.3 * 3^{1/3}$	± 10%	20%
V_i	45.0	± 10%	factor of 4
dV_i/dE (energy dependence)	0.124	± 10%	3%
R_V	$1.75 * 3^{1/3}$	± 10%	factor of 8
a_V	0.593	± 10%	20%
W	0.610	± 10%	5%
dW/dE	0.056	± 10%	3%
R_W	$4.458 * 3^{1/3}$	± 10%	10%
dR_W/dE	$-0.165 * 3^{1/3}$	± 10%	2%
a_W	0.526	± 10%	5%
final-state potential parameters [in eq. (2), p. 59]:			
R_c	$1.3 * 3^{1/3}$	± 10%	20%
R_V	$1.75 * 3^{1/3}$	± 10%	35%
a_V	0.593	± 10%	25%
Q	16.7	± 10%	50%

Figure 1

Energy Level Diagram of the ^{5}He and ^{5}Li Nuclei (Ajzenberg-Selove and Lauritsen 1974), see text, p. 1 and p. 41.

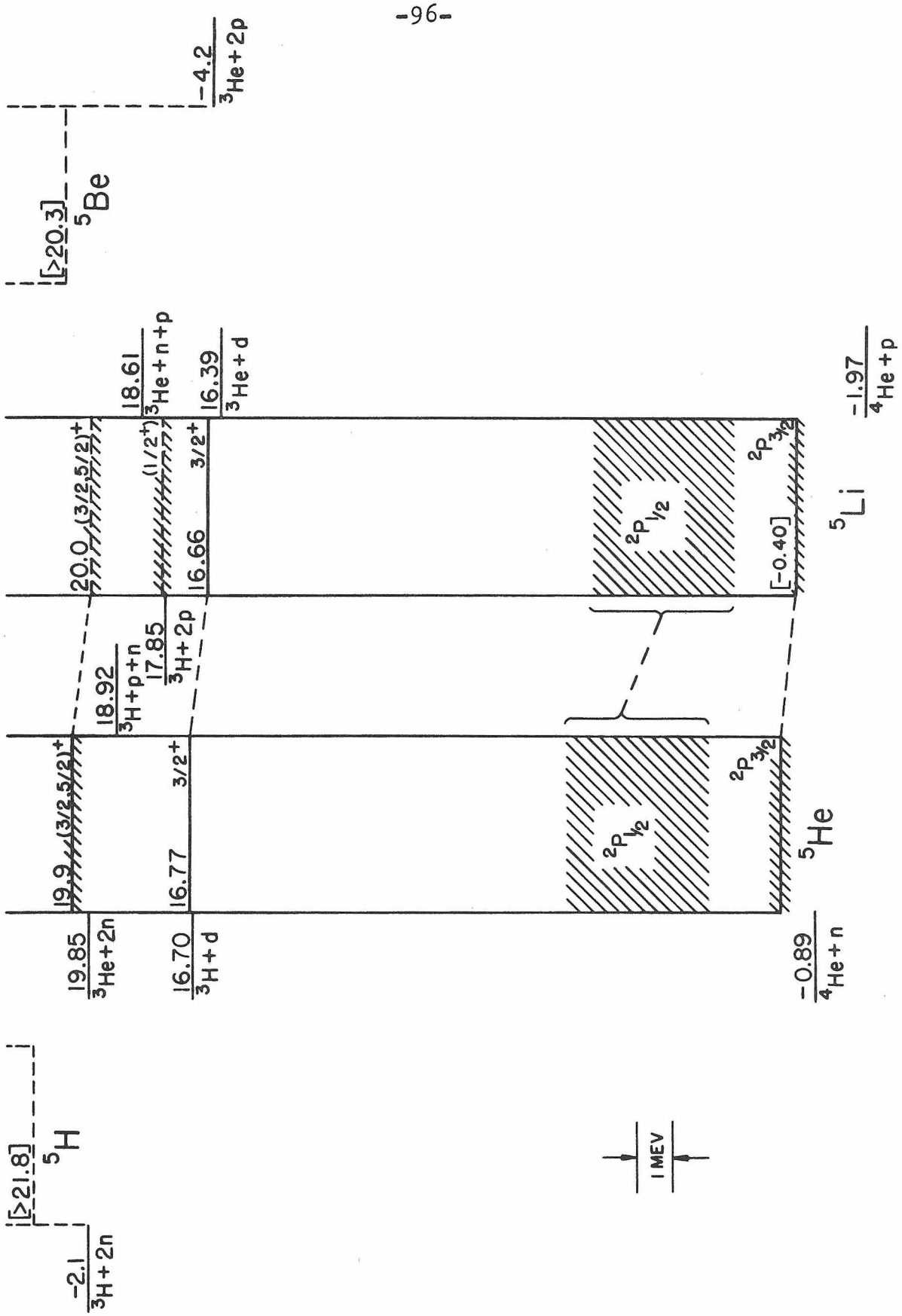
[>21.8]
5H
-2.1
3H+2n
19.85
3He+2n
19.9
(3/2,5/2)+
16.70
3H+d
16.77
3/2+
18.92
3H+p+n
17.85
3H+2p
[>20.3]
5Be
-4.2
3He+2p
18.61
3He+n+p
16.39
3He+d
20.0
(3/2,5/2)+
(1/2+)
3/2+
16.66
2P1/2
2P3/2
[-0.40]
5Li
-1.97
4He+p
2P1/2
2P3/2
5He
-0.89
4He+n
1 MEV

Figure 1

Figure 2

Schematic Diagram of the Target and Detection System

The left diagram shows a vertical section of the target chamber and vacuum system (not to scale). For additional details, see p. 10.

The right diagram shows the detector geometry and the lead shielding (not to scale). For additional details, see p. 11.

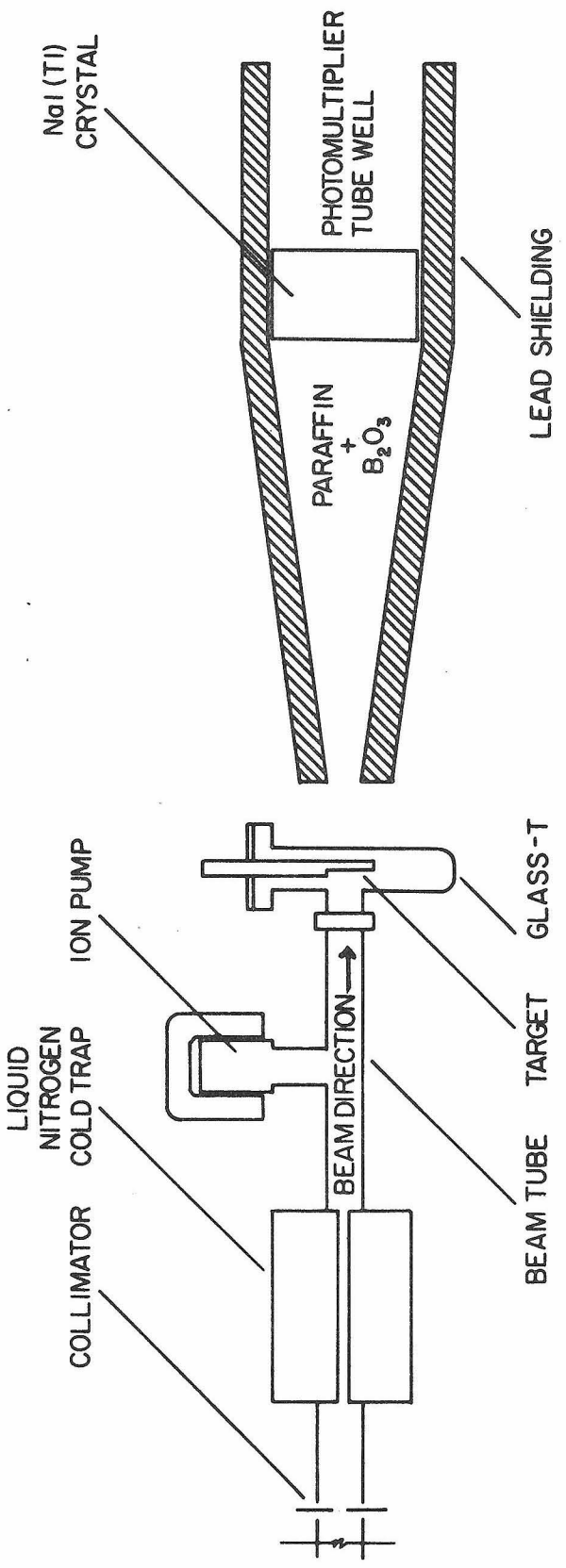
NaI(Tl)
CRYSTAL
PHOTOMULTIPLIER
TUBE WELL
PARAFFIN
+
B_2O_3
LEAD SHIELDING
ION PUMP
GLASS-T
LIQUID
NITROGEN
COLD TRAP
BEAM DIRECTION
TARGET
COLLIMATOR
BEAM TUBE

Figure 2

Figure 3

Electronic Configuration for Measurements of $T(d,\gamma)^5He$ and $T(p,\gamma)^5He$ Yields. See text, p. 12.

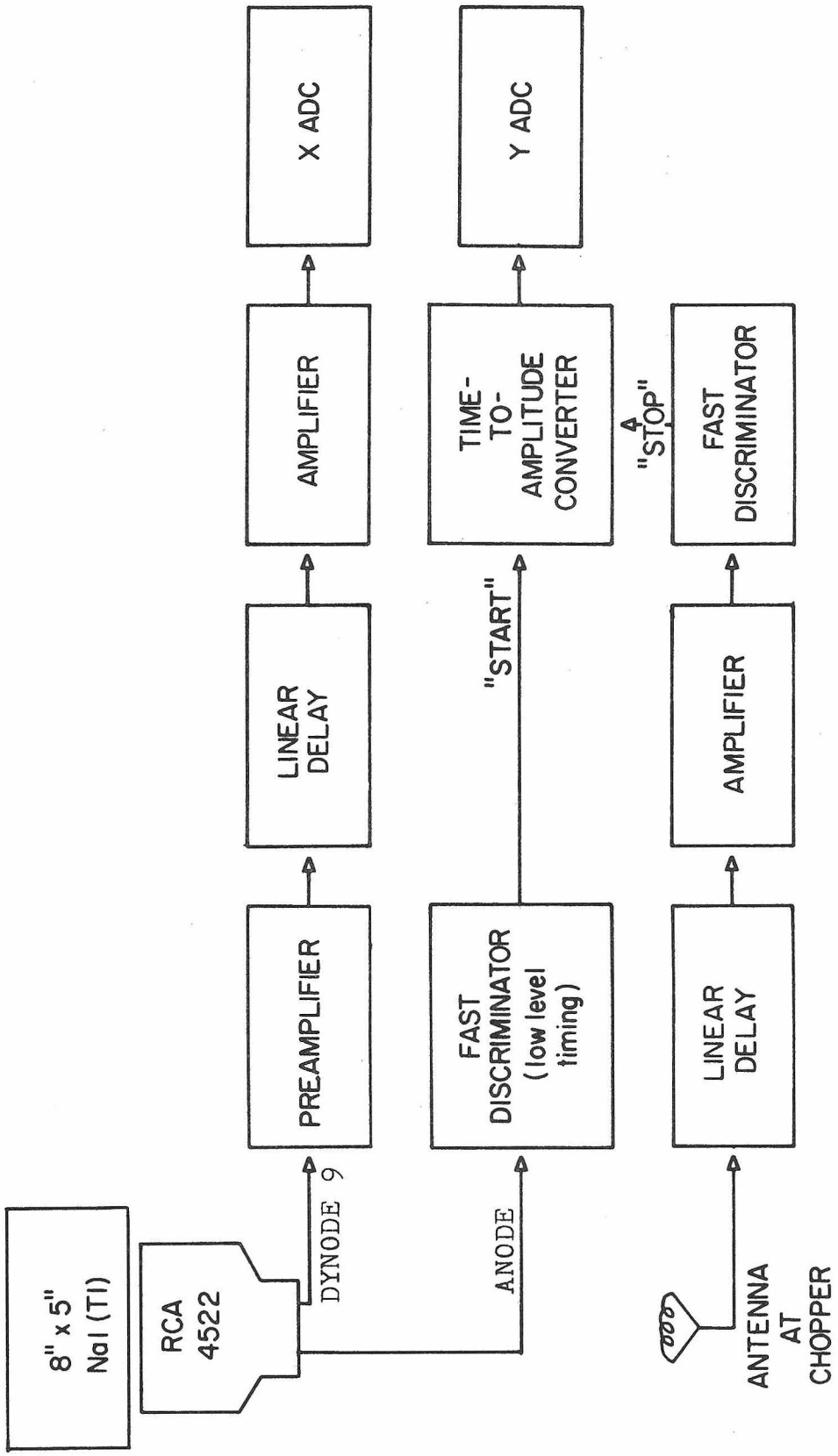
8" x 5"
NaI (Tl)
RCA
4522
DYNODE 9
ANODE
PREAMPLIFIER
FAST
DISCRIMINATOR
(low level
timing)
LINEAR
DELAY
"START"
"STOP"
LINEAR
DELAY
AMPLIFIER
AMPLIFIER
TIME-
TO-
AMPLITUDE
CONVERTER
FAST
DISCRIMINATOR
X ADC
Y ADC
ANTENNA
AT
CHOPPER

Figure 3

Figure 4

21 MeV Standard Spectrum for an 8" x 5" NaI(Tℓ) Crystal

This pulse height spectrum for a monochromatic γ-ray was measured with the $T(p,\gamma)^4He$ reaction (Q = 19.8 MeV) at E_p^{lab} = 1.5 MeV. The dots represent the data with the background subtracted. The solid line represents the nonlinear least-squares fit described in Appendix 2. The dashed line represents an estimate of the low energy background. See text, p. 16 and Appendix 2.

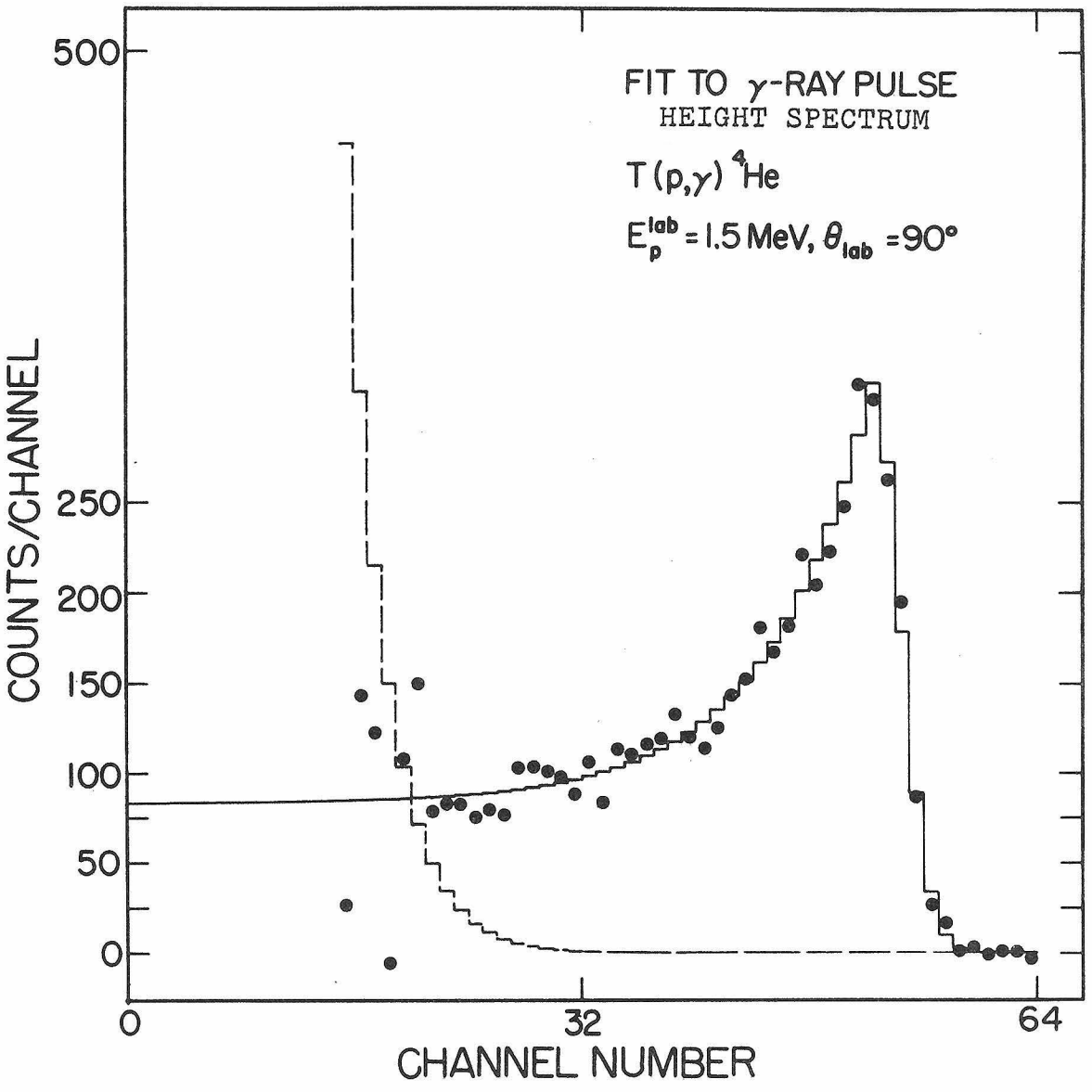
FIT TO γ-RAY PULSE
HEIGHT SPECTRUM
T(p,γ) 4He
E_p^lab = 1.5 MeV, θ_lab = 90°
COUNTS/CHANNEL
500
250
200
150
100
50
0
0
32
64
CHANNEL NUMBER

Figure 4

Figure 5

Pulse Height (Energy) of Gamma Rays from the $T(d,\gamma_0)^5He$ and $T(p,\gamma)^4He$ Reactions

These spectra are obtained from the two-dimensional spectra by summing counts over the time channels corresponding to the arrival of gamma-rays from the target, and subtracting the energy spectrum of the time-independent background obtained from the same two-dimensional spectrum. Channel zero corresponds to zero gamma-ray energy; channel 64 to about 30 MeV. See text, p. 16.

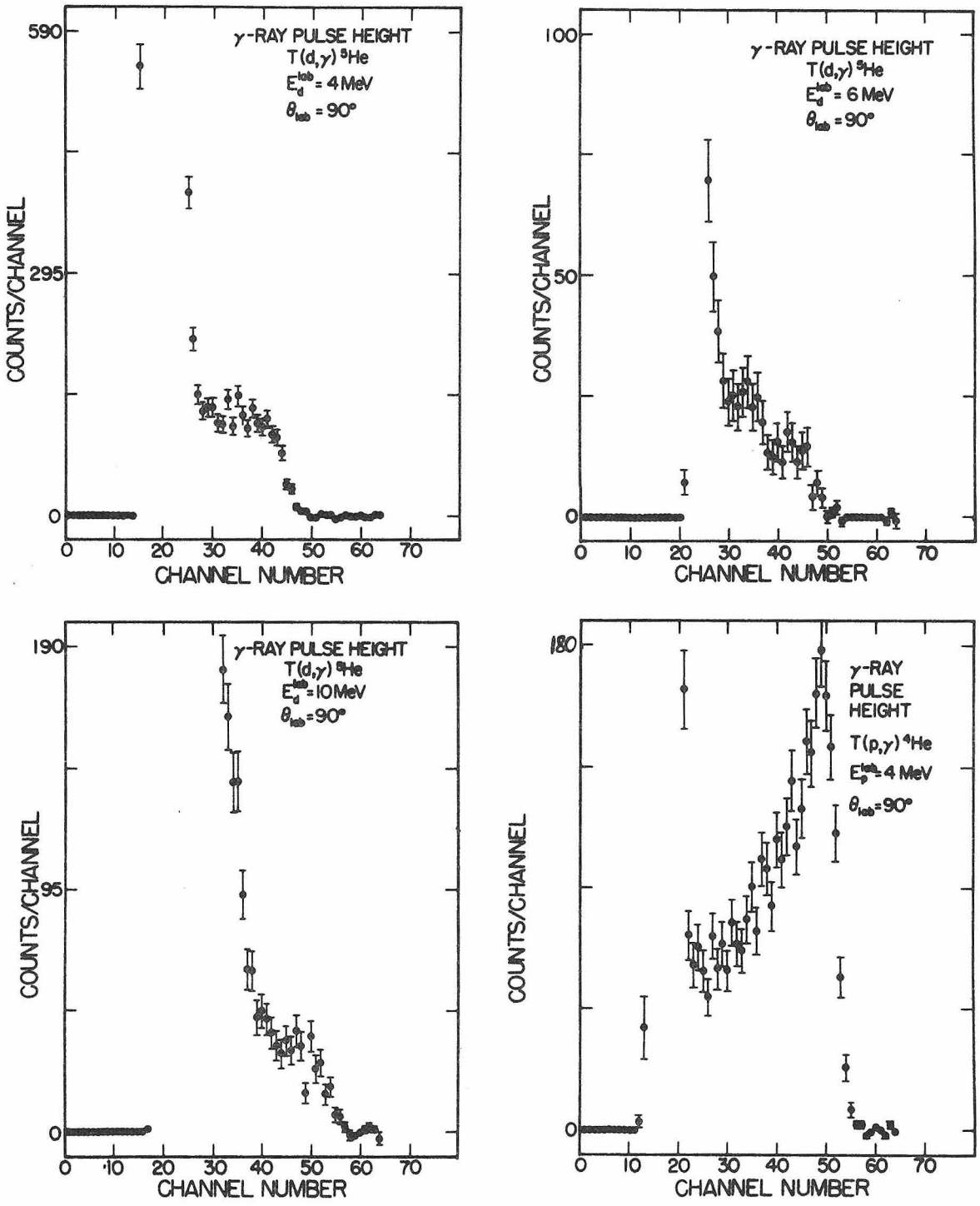
γ-RAY PULSE HEIGHT
T(d,γ)⁵He
E_d^lab = 4 MeV
θ_lab = 90°
590
295
0
COUNTS/CHANNEL
0 10 20 30 40 50 60 70
CHANNEL NUMBER
γ-RAY PULSE HEIGHT
T(d,γ)⁵He
E_d^lab = 6 MeV
θ_lab = 90°
100
50
0
COUNTS/CHANNEL
0 10 20 30 40 50 60 70
CHANNEL NUMBER
γ-RAY PULSE HEIGHT
T(d,γ)⁵He
E_d^lab = 10 MeV
θ_lab = 90°
190
95
0
COUNTS/CHANNEL
0 10 20 30 40 50 60 70
CHANNEL NUMBER
γ-RAY
PULSE
HEIGHT
T(p,γ)⁴He
E_p^lab = 4 MeV
θ_lab = 90°
180
0
COUNTS/CHANNEL
0 10 20 30 40 50 60 70
CHANNEL NUMBER

Figure 5

Figure 6

Time-of-Flight Spectra for 12 MeV Events from the $T(d,\gamma_0)^5He$ Reaction

These spectra were obtained from the two-dimensional spectra by summing counts over the energy channels corresponding to the gamma-ray energy (E_γ^o) of the transitions to the ground state of ^5He. For E_d^{lab} = 12 MeV, E_γ^o = 23.9 MeV. The region of summation is taken from 0.8 E_γ^o to 1.1 E_γ^o. Time increases to the left. The energy calibration is approximately 0.5 nsec/channel. The peak between channels 20 and 30 corresponds to the γ-rays and has a FWHM of approximately 3 nsec. The peak on the left corresponds to prompt neutrons from the $T(d,n)^4He$ reaction. The peaks are separated by about 10 nsec, corresponding to the difference in flight times for neutrons and gamma rays. See text, p. 17.

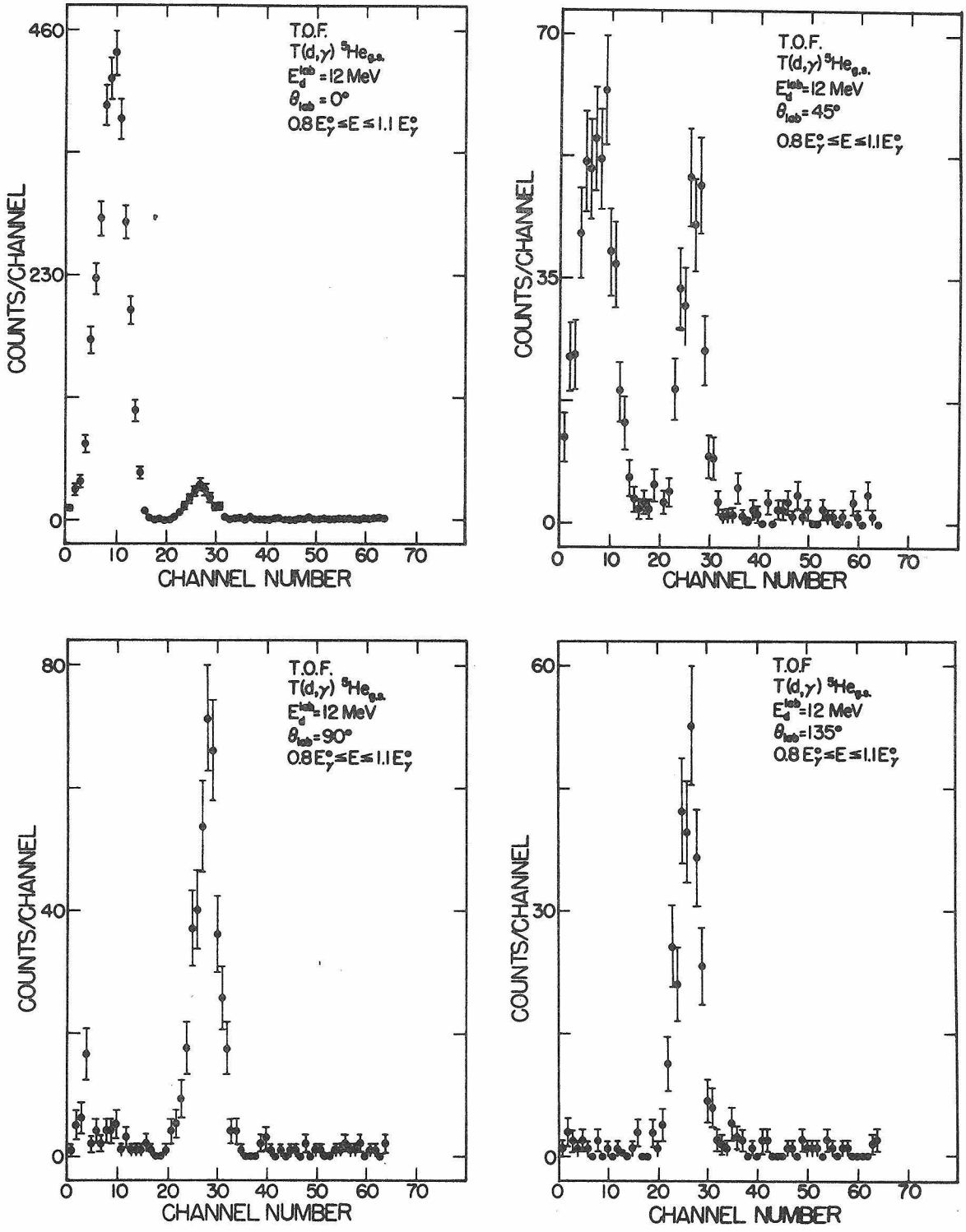
T.O.F.
T(d,γ) 5He g.s.
Ed lab = 12 MeV
θlab = 0°
0.8 Eγ° ≤ E ≤ 1.1 Eγ°
COUNTS/CHANNEL
CHANNEL NUMBER
T.O.F.
T(d,γ) 5He g.s.
Ed lab = 12 MeV
θlab = 45°
0.8 Eγ° ≤ E ≤ 1.1 Eγ°
COUNTS/CHANNEL
CHANNEL NUMBER
T.O.F.
T(d,γ) 5He g.s.
Ed lab = 12 MeV
θlab = 90°
0.8 Eγ° ≤ E ≤ 1.1 Eγ°
COUNTS/CHANNEL
CHANNEL NUMBER
T.O.F
T(d,γ) 5He g.s.
Ed lab = 12 MeV
θlab = 135°
0.8 Eγ° ≤ E ≤ 1.1 Eγ°
COUNTS/CHANNEL
CHANNEL NUMBER

Figure 6

Figure 7

The 90° Differential Cross Section for the $T(d,\gamma_0)^5He$ Reaction

The error bars represent the statistical uncertainty only.

See text, p. 23 and p. 28.

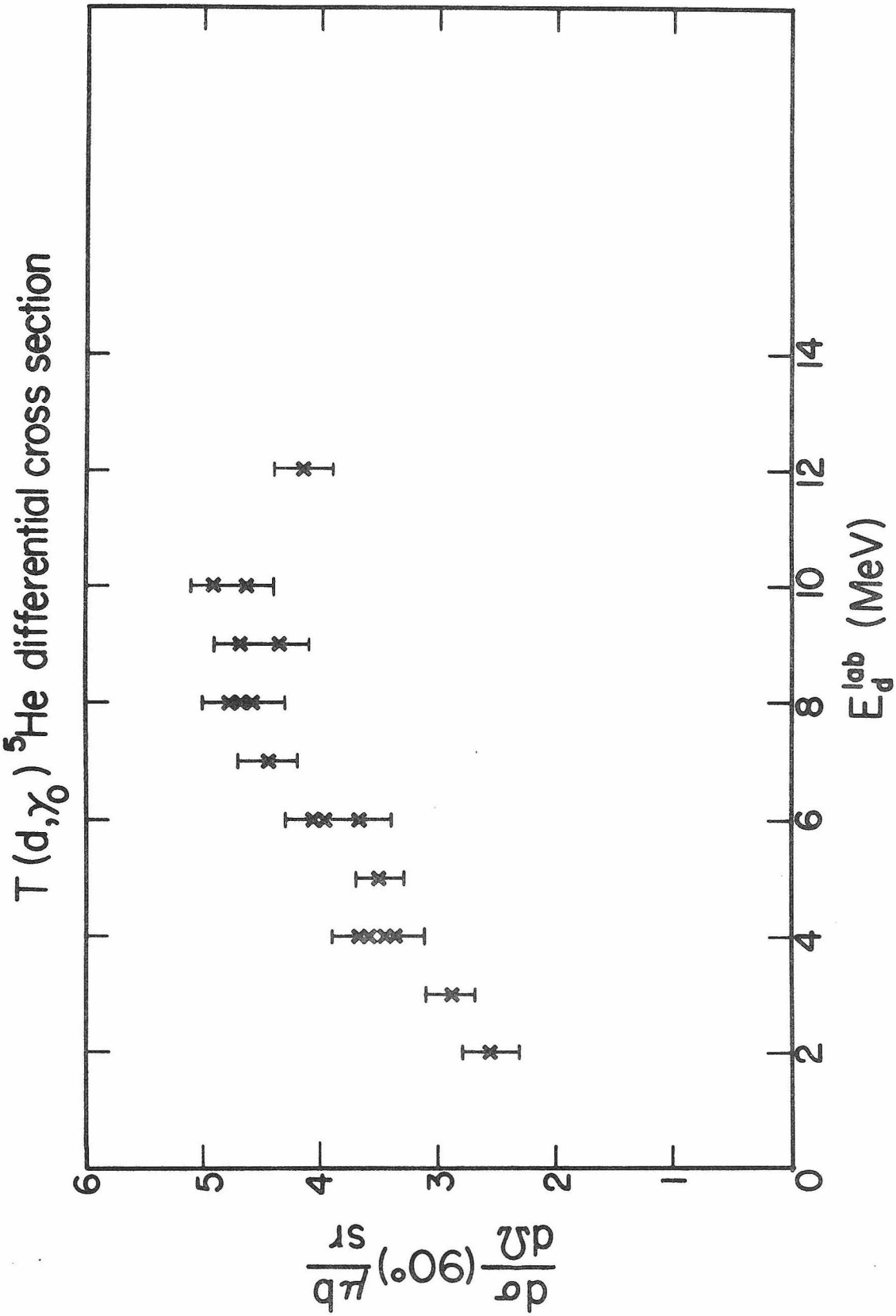
T (d,γ0) 5He differential cross section
dσ/dΩ (90°) μb/sr
0
1
2
3
4
5
6
2
4
6
8
10
12
14
E_d^lab (MeV)

Figure 7

Figure 8

Comparison of the Cross Section and Angular Distribution of the $T(d,\gamma)^5He$ and $D(^3He,\gamma)^5Li$ Reactions

The crosses correspond to the $T(d,\gamma)^5He$ reaction.

The dots represent the $D(^3He,\gamma)^5Li$ data taken from King et al. (1972).

The upper diagram gives the 90° laboratory differential cross section. See text, p. 23 and Figure 7.

The lower diagram gives the energy dependence of A_2/A_o where A_2 and A_o are the coefficients of P_2 and P_o in the Legendre fits. See text, p. 27.

The data are plotted as a function of the excitation energy in the compound nucleus, $E_x(^5A)$.

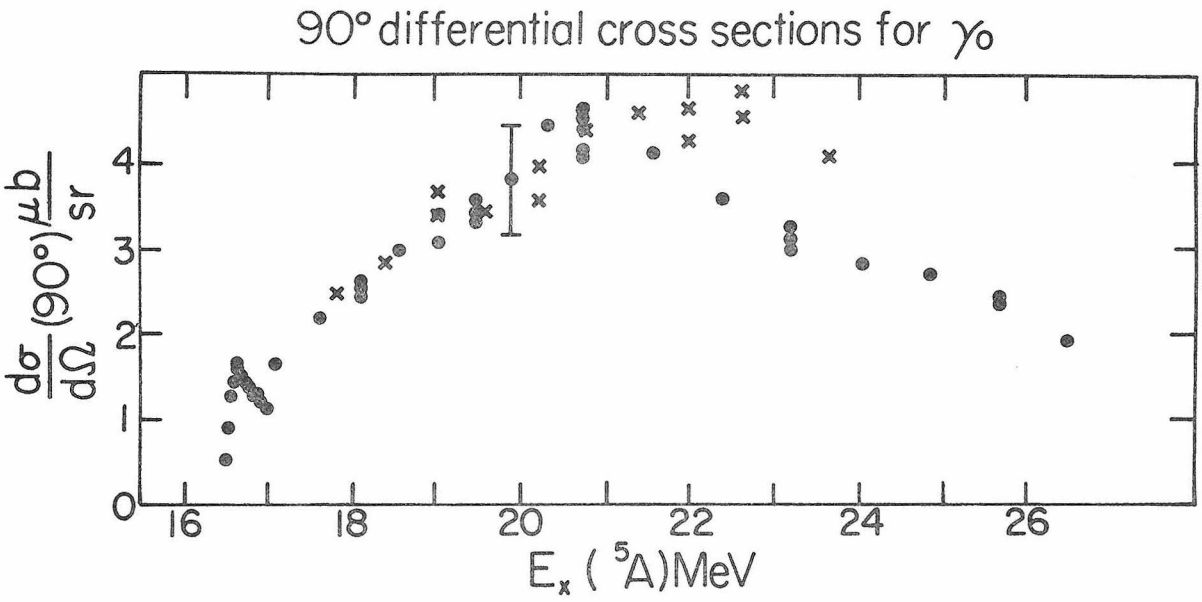
90° differential cross sections for γ_0
$\frac{d\sigma}{d\Omega}(90°)\frac{\mu b}{sr}$
0
1
2
3
4
16
18
20
22
24
26
E_x (^{5}A) MeV

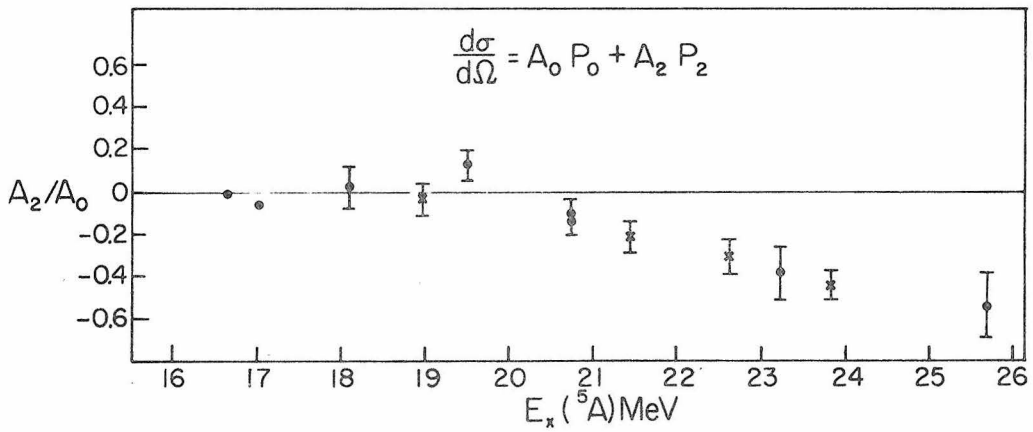
$\frac{d\sigma}{d\Omega} = A_0 P_0 + A_2 P_2$
A_2/A_0
0.6
0.4
0.2
0
-0.2
-0.4
-0.6
16
17
18
19
20
21
22
23
24
25
26
E_x (^{5}A) MeV

Figure 8

Figure 9

The $T(d,\gamma)^5He$ and $T(p,\gamma)^4He$ Angular Distributions

Y_{CM}^{NORM} are the yields per micro-Coulomb divided by the detection efficiency ε and transformed to the center-of mass coordinate system. The yields are plotted versus the angle θ_{CM}, measured with respect to the direction of the incident beam and transformed to the CM system.

The solid curves indicate the Legendre fits with P_o and P_2. See text, p. 26.

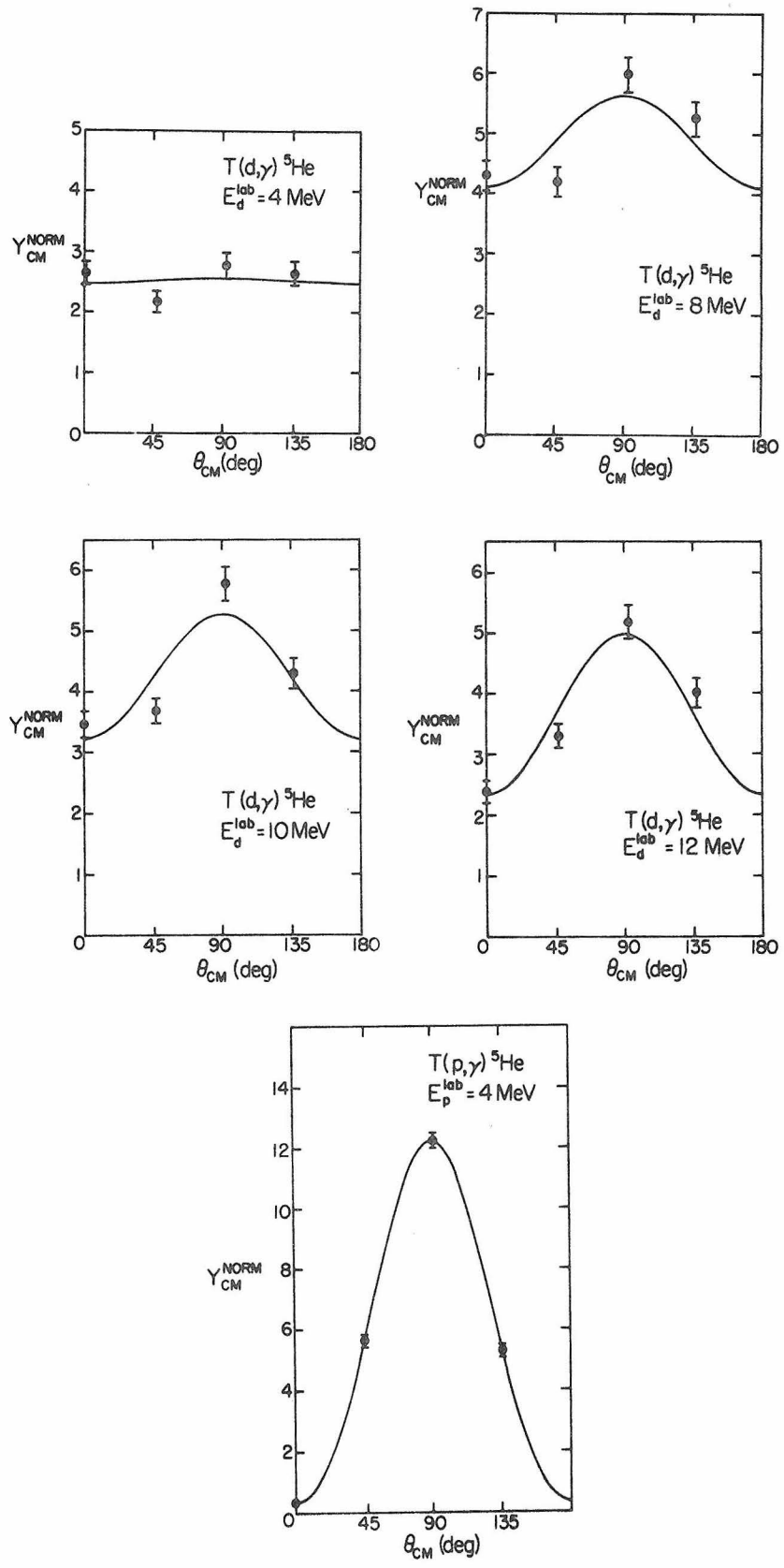
T(d,γ) ⁵He
E_d^lab = 4 MeV
T(d,γ) ⁵He
E_d^lab = 8 MeV
T(d,γ) ⁵He
E_d^lab = 10 MeV
T(d,γ) ⁵He
E_d^lab = 12 MeV
T(p,γ) ⁵He
E_p^lab = 4 MeV
Y_CM^NORM
θ_CM (deg)

Figure 9

Figure 10

T + d Elastic Scattering Differential Cross Sections

The dots represent the data from Tombrello (1967) and Stratton (1952).

The solid lines represent the cross sections derived from the optical model potentials given on page 56. See also text, p. 63.

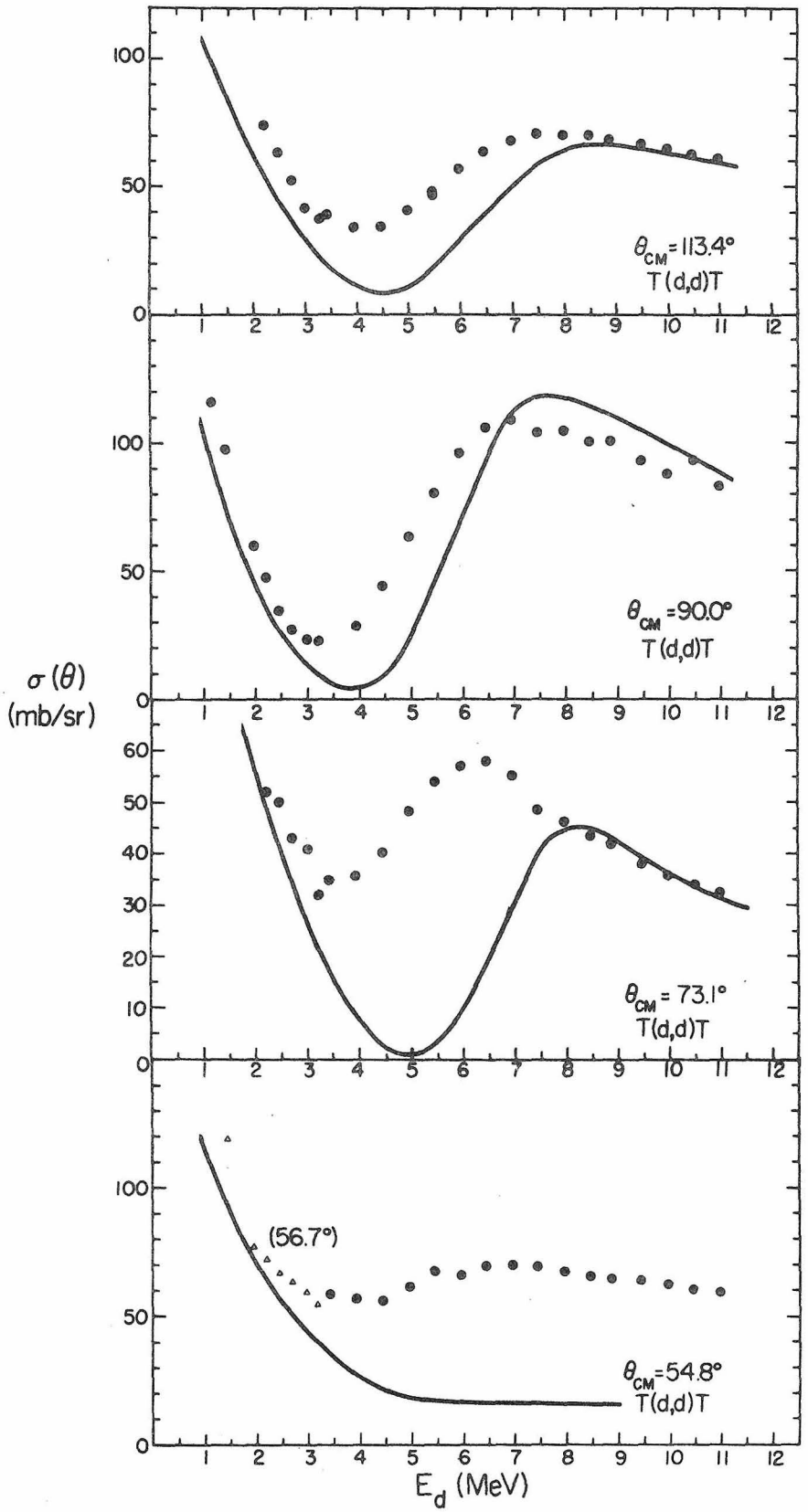
σ (θ)
(mb/sr)
θCM = 113.4°
T(d,d)T
θCM = 90.0°
T(d,d)T
θCM = 73.1°
T(d,d)T
(56.7°)
θCM = 54.8°
T(d,d)T
Ed (MeV)

Figure 10

Figure 11

The Experimental and Calculated Total $T(d,\gamma)^5He_{g.s.}$ Cross Sections

The data are derived from the 90° measurements between 2 and 12 MeV, and from the extrapolated A_2/A_0 coefficients determined at 4, 8, 10 and 12 MeV. See text, p.27.

The solid curve represents the E1 direct capture cross section calculated on the basis of a bound ground state of ^5He. The overall normalization has not been adjusted. The broken lines represent the partial cross sections from initial S and D waves. See text, p.69.

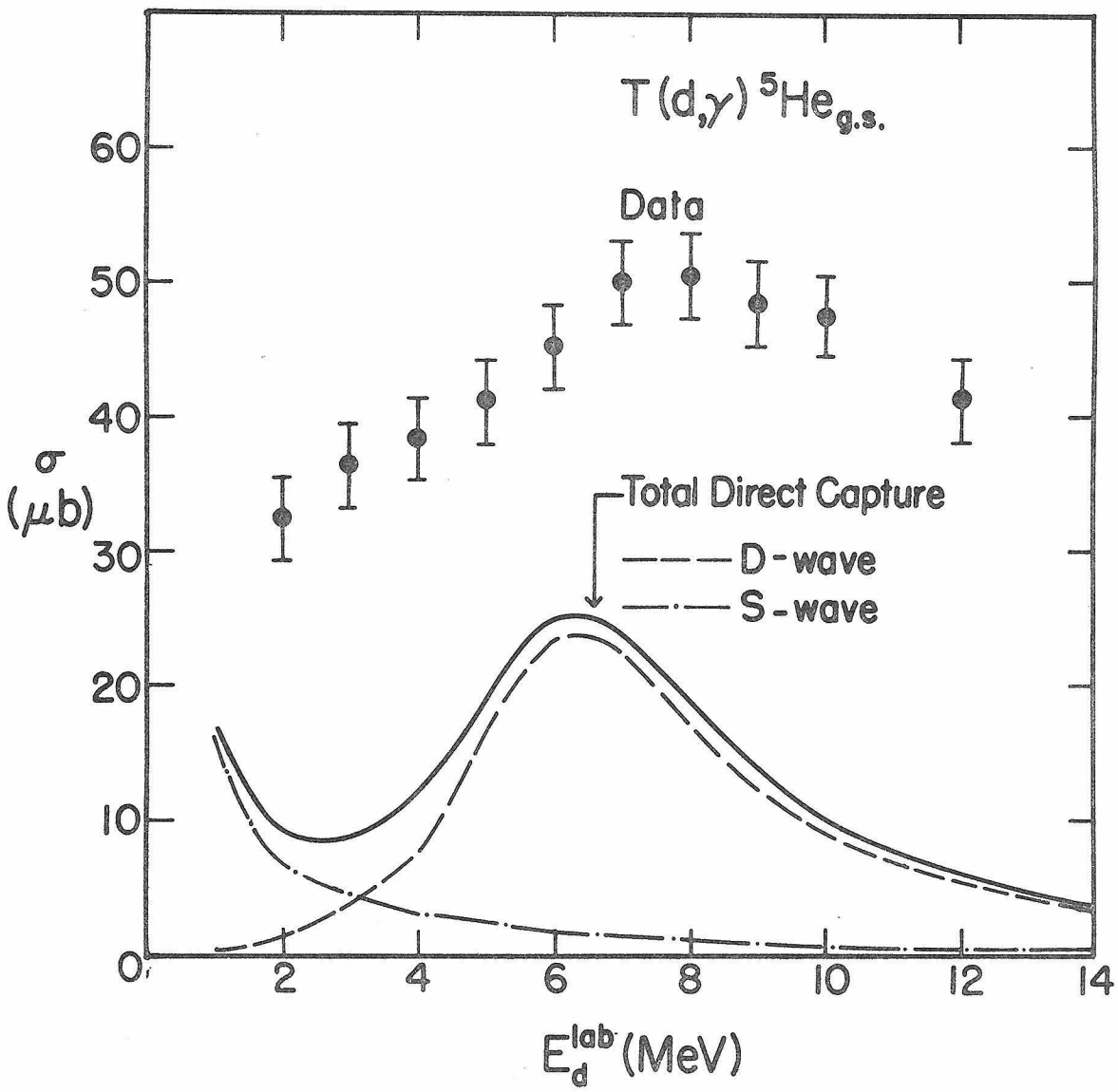
T(d,γ) 5He g.s.
Data
Total Direct Capture
D-wave
S-wave
σ (μb)
60
50
40
30
20
10
0
2
4
6
8
10
12
14
E_d^lab (MeV)

Figure 11